

Control of Low-Inertia Power Systems

Florian Dörfler¹ and Dominic Groß²

¹Automatic Control Laboratory, ETH Zurich, Zurich, Switzerland, 8092; email: dorfler@ethz.ch

²Electrical and Computer Engineering, University of Wisconsin-Madison, Madison, United States, WI 53706; email: dominic.gross@wisc.edu

Xxxx. Xxx. Xxx. Xxx. YYYY. AA:1–30

[https://doi.org/10.1146/\(\(please add article doi\)\)](https://doi.org/10.1146/((please add article doi)))

Copyright © YYYY by Annual Reviews.
All rights reserved

Keywords

Power systems control, power electronics control, low-inertia systems, grid-forming control, dynamic virtual power plant

Abstract

Electric power systems are undergoing an unprecedented transition from fossil fuel-based power plants to low-inertia systems that predominantly rely on power electronics and renewable energy resources. This article reviews the resulting modeling and control challenges, both at the device- and system-level, and predominantly focuses on novel aspects or classical concepts that have to be revised in light of the transition to low-inertia systems. To this end, we survey the literature on modeling of low-inertia systems, control of grid-connected power converters, and discuss the frequency dynamics of low-inertia systems. Moreover, we discuss system-level services from a control perspective. Overall, we conclude that the system-theoretic mind set is essential to bridge different research communities and understand the complex interactions of power electronics, electric machines, and their controls in large-scale low-inertia power systems.

1. INTRODUCTION

The future electric power system is envisioned to be both sustainable and highly resilient. An ever-increasing share of conventional fossil fuel-based power plants is being replaced by renewable energy resources. This transition to a sustainable system involves the major challenge of replacing bulk generation interfaced with synchronous machines by distributed generation primarily interfaced with power electronics. Unlike other past evolutions of the electric power system, these unprecedented changes affect its very core, namely the power generation and conversion technology: from conventional rotational power generation based on synchronous machines towards power converter-interfaced generation and conversion, as in the case of renewable energy sources, battery storage, or high-voltage dc links interconnecting different synchronous areas.

This transition poses major challenges to the operation, control, stability, and resilience of the power system due to (i) the loss of rotational kinetic energy in synchronous machines whose inertia acts a safeguard against disturbances; (ii) the loss of the stable and robust nonlinear synchronization mechanism which is physically inherent to rotational generation; (iii) the loss of robust frequency and voltage control as well as stabilizing ancillary services provided by synchronous machines; (iv) all of which is paired with the variability and intermittency of renewable generation.

We refer to the set of recent surveys, tutorials, and magazine articles (1, 2, 3, 4, 5, 6, 7, 8, 9, 10, 11, 12, 13) illustrating the various challenges of future so-called *low-inertia power systems* from the power systems, power electronics, and controls' perspectives. A universal conclusion is that the modeling, stability analysis, simulation, and control of low-inertia systems have to be revisited, and many thus far canonical concepts have to be questioned. Further, it leads to the confluence of the (thus far mostly disjoint) power systems and power electronics communities whose interactions are facilitated by means of systems and control theory acting as a common lingua franca.

Here we take the systems and controls perspective and review the modeling and control challenges of low-inertia power systems as well as some first solutions that have been put forward. We will cover both device-level and system-level aspects. We do not aim to be comprehensive in our scope, but we focus predominantly either on novel aspects or traditional concepts which need to be revised in low-inertia systems. Inevitably this article is coloured and biased by our own research interests and experiences and does not present all viewpoints and facets on the topic of low-inertia power systems.

The remainder of the article is organized as follows. Section 2 reviews salient elements of low-inertia systems and their models. Section 3 discusses the control of grid-connected converters. Section 4 discusses the frequency dynamics of low-inertia systems. Finally, Section 5 discusses the system-level services and controls aspects.

2. SALIENT ELEMENTS OF LOW-INERTIA SYSTEMS & THEIR MODELS

In this section we briefly recap the modeling of ac power systems with a particular focus on salient elements of future low-inertia systems, i.e., time-domain models of the networks circuitry and device-level models of synchronous machines and power converters. For further reading we refer to (14, 15, 16) for relevant textbooks covering the modeling of power systems and grid-connected power converters.

2.1. Three-Phase AC Power System

A power system broadly speaking consists of generation, load, and the circuitry (i.e., the power network) interconnecting them. We begin with the latter, and refer to (17, 18, 19) and references therein for network-theoretic or Port-Hamiltonian modeling perspectives.

2.1.1. Power network model. We model the network as a *graph* with nodes (or buses) \mathcal{V} , edges (or lines or branches) $\mathcal{E} \subset \mathcal{V} \times \mathcal{V}$, and oriented node-edge *incidence matrix* $B \in \mathbb{R}^{|\mathcal{V}| \times |\mathcal{E}|}$

$$B_{ie} = \begin{cases} +1, & \text{if the edge } e \text{ is } (i, j) \text{ for some } j, \\ -1, & \text{if the edge } e \text{ is } (j, i) \text{ for some } j, \\ 0, & \text{otherwise.} \end{cases}$$

For every bus $i \in \mathcal{V}$ we define a *potential* (or nodal voltage) $\mathbf{v}_i \in \mathbb{R}^3$ and an *exogenous current injection* $\mathbf{I}_i \in \mathbb{R}^3$. Likewise, for every branch $e \in \mathcal{E}$ we define an oriented *current flow* $\mathbf{i}_e \in \mathbb{R}^3$ and an oriented *voltage drop* $\mathbf{u}_e \in \mathbb{R}^3$. All currents and voltages are *three-phase* signals with components labeled *abc*, e.g., $\mathbf{v}_i = [v_{i,a} \ v_{i,b} \ v_{i,c}]^\top$. We will further discuss the signal space in Section 2.1.2. *Kirchhoff's voltage and current laws* relate these signals as

$$\mathbf{I} = \mathbf{B}\mathbf{i} \quad \text{and} \quad \mathbf{u} = \mathbf{B}^\top \mathbf{v}, \quad 1.$$

where we defined the shorthands $\mathbf{B} := (B \otimes \mathcal{I}_3)$, $\mathbf{I} := (\mathbf{I}_1, \dots, \mathbf{I}_{|\mathcal{V}|})$, $\mathbf{v} := (\mathbf{v}_1, \dots, \mathbf{v}_{|\mathcal{V}|})$, $\mathbf{u} := (\mathbf{u}_1, \dots, \mathbf{u}_{|\mathcal{E}|})$, and $\mathbf{i} := (\mathbf{i}_1, \dots, \mathbf{i}_{|\mathcal{E}|})$, where \mathcal{I}_3 denotes the 3×3 identity matrix.

We further complement Kirchhoff's laws through *constitutive relations* (such as Ohm's law) relating \mathbf{i}_e and \mathbf{u}_e for any branch $e \in \mathcal{E}$. The three typical constitutive relations are

- *resistive*: $\mathbf{u}_e = r_e \mathbf{i}_e$, where $r_e > 0$ is a resistance;
- *inductive*: $l_e \frac{d}{dt} \mathbf{i}_e = \mathbf{u}_e$, where $l_e > 0$ is an inductance; and
- *capacitive*: $c_e \frac{d}{dt} \mathbf{u}_e = \mathbf{i}_e$, where $c_e > 0$ is a capacitance.

Observe that here we have implicitly assumed that the circuitry is *symmetric*, i.e., r_e , l_e , and c_e are scalar parameters rather than general 3×3 matrices accounting for non-uniformities and interactions among phases. This assumption is valid for high-voltage transmission systems commonly considered in the literature on low-inertia systems. Finally, power system specifications are often given in units power. Loosely speaking, power is the product of current and voltage. However, there are many co-existing definitions of power, especially for reactive power (20, 21). It makes sense to define power in particular coordinates attached to a three-phase system, which are introduced in Section 2.1.2 below.

2.1.2. Three-phase signals: specifications and coordinate frames. Consider a *three-phase* circuit signal $\mathbf{x}_{abc} = [x_a \ x_b \ x_c]^\top \in \mathbb{R}^3$, e.g., any nodal or branch voltage/current. Three-phase signals in power transmission systems are not arbitrary but (due to three-wire transmission, three-phase generation and conversion, and control) but

- *periodic* with zero average: $\frac{1}{T} \int_0^T x_i(\tau) d\tau = 0$ for some $T > 0$ and for all $i \in \{a, b, c\}$;
- *balanced*: $\mathbf{x}_{abc} = A(t) \begin{bmatrix} \sin(\delta(t)) \\ \sin(\delta(t) - \frac{2\pi}{3}) \\ \sin(\delta(t) + \frac{2\pi}{3}) \end{bmatrix}$ for some time-varying angle $\delta(t)$ and non-negative amplitude $A(t)$ so that $x_a(t) + x_b(t) + x_c(t) = 0$ for all $t \geq 0$; and

- *synchronous* (in steady state) with constant frequency ω : $\mathbf{x}_{abc} = A \begin{bmatrix} \sin(\delta + \omega t) \\ \sin(\delta + \omega t - \frac{2\pi}{3}) \\ \sin(\delta + \omega t + \frac{2\pi}{3}) \end{bmatrix}$ for some constant amplitude A and angle δ .

For the problems considered in this article, it is fair to assume that all signals are periodic and balanced, and the role of analysis and control design is to certify stability of synchronous solutions, where all signals in the circuit have common synchronous frequency ω .

Many coordinate frames and representations have been introduced to study three-phase signals; see the sidebar entitled *Coordinate frames for three-phase signals* and, e.g., (22). Throughout this text we will work in a $dq0$ frame induced by the orthonormal (i.e., power invariant) *Park transform* attached to the nominal ac network frequency ω_0 , e.g., $\omega_0 = 2\pi \cdot 50\text{Hz}$ or $\omega_0 = 2\pi \cdot 60\text{Hz}$, we drop the zero-component, and we generally omit the subscripts abc , $\alpha\beta$, dq , and so on. The reader may convince her/himself that in such a coordinate frame the constitutive relations for inductor and resistor change to

$$l_e \frac{d}{dt} \mathbf{i}_e = -\mathbf{J}\omega_0 l_e \mathbf{i}_e + \mathbf{u}_e \quad \text{and} \quad c_e \frac{d}{dt} \mathbf{u}_e = -\mathbf{J}\omega_0 c_e \mathbf{u}_e + \mathbf{i}_e,$$

where the 90° rotation matrix $\mathbf{J} = \begin{bmatrix} 0 & -1 \\ 1 & 0 \end{bmatrix}$ is the analogue of the imaginary unit $j = \sqrt{-1}$. This analogy is deliberate since $\mathbf{J}^2 = -\mathcal{I}$, $\mathbf{J}^\top = -\mathbf{J}$, and the terms $\mathbf{J}\omega_0 l_e$ and $\mathbf{J}\omega_0 c_e$ recover the familiar complex-valued formulations of inductive and capacitive impedances.

Among the many definitions of active and reactive power, we use *instantaneous power* (20, 22). Namely, for a current \mathbf{i} and voltage \mathbf{v} at the same bus, *active power* is defined as

$$p = \mathbf{i}^\top \mathbf{v}, \tag{2}$$

i.e., an inner product, and *reactive power* is defined by the cross product written as

$$q = \mathbf{i}^\top \mathbf{J} \mathbf{v} \tag{3}$$

equal to positive sequence powers of standard three-phase phasor model.

2.1.3. Line & load dynamics. We specify the exogenous current injection at node i as

$$\mathbf{I}_i = \mathbf{I}_{i,g} - \mathbf{I}_{i,\text{load}} - \mathbf{I}_{i,\text{charge}} \tag{4}$$

accounting for the dynamic contribution of generation, loads, and line charging. Generation will be specified in Section 2.2, and we now focus on the latter and the constitutive relations.

Power system lines are typically specified by the Π -model; see Figure 1. A series of resistive and inductive elements models the inductance and losses of line $e \in \mathcal{E}$ as

$$l_e \frac{d}{dt} \mathbf{i}_e = -(r_e \mathcal{I} + \mathbf{J}\omega_0 l_e) \mathbf{i}_e + \mathbf{u}_e. \tag{5}$$

Lines range from dominantly inductive (in high-voltage transmission) to being equally inductive and resistive (in low-voltage distribution). Further, the charging effect of the line is modeled by a capacitive connection to the ground on either end of the line, i.e.,

$$c_i \frac{d}{dt} \mathbf{v}_i = \mathbf{I}_{i,\text{charge}}. \tag{6}$$

We will not discuss the detailed modeling of loads and refer the reader to (23, 15). For the considered problems, it is typically sufficient to model loads on an aggregate level as

Coordinate frames for three-phase signals

Consider a periodic and balanced three-phase signal

$$\mathbf{x}_{abc} = \begin{bmatrix} x_a \\ x_b \\ x_c \end{bmatrix} = A \begin{bmatrix} \sin(\delta) \\ \sin(\delta - \frac{2\pi}{3}) \\ \sin(\delta + \frac{2\pi}{3}) \end{bmatrix},$$

where we omitted the dependence of \mathbf{x}_{abc} , A , and δ on time. Balancedness applies that \mathbf{x}_{abc} is orthogonal to $[1 \ 1 \ 1]$. Consider the orthonormal *Clarke transform* $\mathbf{T}_{\alpha\beta 0}$: $\mathbf{x}_{abc} \rightarrow \mathbf{x}_{\alpha\beta 0}$ removing the balanced subspace:

$$\mathbf{T}_{\alpha\beta 0} = \sqrt{\frac{2}{3}} \begin{bmatrix} 1 & -\frac{1}{2} & -\frac{1}{2} \\ 0 & \frac{\sqrt{3}}{2} & -\frac{\sqrt{3}}{2} \\ \frac{1}{\sqrt{2}} & \frac{1}{\sqrt{2}} & \frac{1}{\sqrt{2}} \end{bmatrix}$$

The resulting coordinate frame is denoted by $\alpha\beta 0$, and the signal $\mathbf{x}_{\alpha\beta 0} = \mathbf{T}_{\alpha\beta 0}\mathbf{x}_{abc}$ satisfies

$$\mathbf{x}_{\alpha\beta 0} = \begin{bmatrix} x_\alpha \\ x_\beta \\ x_0 \end{bmatrix} = \sqrt{\frac{3}{2}}A \begin{bmatrix} \sin(\delta) \\ -\cos(\delta) \\ 0 \end{bmatrix}$$

Next, consider the orthonormal *Park transform* $\mathbf{T}_{dq0}(\theta)$: $\mathbf{x}_{\alpha\beta 0} \rightarrow \mathbf{x}_{dq0}$ into a rotating frame with angle θ

$$\mathbf{T}_{dq0}(\theta) = \sqrt{\frac{2}{3}} \begin{bmatrix} \cos(\theta) & -\sin(\theta) & 0 \\ \sin(\theta) & \cos(\theta) & 0 \\ 0 & 0 & 1 \end{bmatrix}.$$

The resulting coordinate frame is denoted by $dq0$, and the signal $\mathbf{x}_{dq0} = \mathbf{T}_{dq0}(\theta)\mathbf{x}_{\alpha\beta 0}$ satisfies

$$\mathbf{x}_{dq0} = \begin{bmatrix} x_d \\ x_q \\ x_0 \end{bmatrix} = \sqrt{\frac{3}{2}}A \begin{bmatrix} \sin(\delta + \theta) \\ -\cos(\delta + \theta) \\ 0 \end{bmatrix} \stackrel{\theta = -\delta}{=} \sqrt{\frac{3}{2}}A \begin{bmatrix} 0 \\ -1 \\ 0 \end{bmatrix}.$$

The component x_0 is normally discarded in a balanced system, and the remaining \mathbf{x}_{dq} coordinates are denoted by a phasor $\sqrt{\frac{3}{2}}A \begin{bmatrix} \sin(\delta + \theta) \\ -\cos(\delta + \theta) \end{bmatrix}$ or in complex coordinates $\sqrt{\frac{3}{2}}A e^{j(\delta - \theta)}$. The overall transform is

$$\mathbf{T}_{dq0} \cdot \mathbf{T}_{\alpha\beta 0} = \sqrt{\frac{2}{3}} \begin{bmatrix} \cos(\theta) & \cos(\theta + \frac{2\pi}{3}) & \cos(\theta - \frac{2\pi}{3}) \\ \sin(\theta) & \sin(\theta + \frac{2\pi}{3}) & \sin(\theta - \frac{2\pi}{3}) \\ \frac{\sqrt{2}}{2} & \frac{\sqrt{2}}{2} & \frac{\sqrt{2}}{2} \end{bmatrix}.$$

mere shunt resistances r_i (sometimes also inductances) or sinks drawing constant current

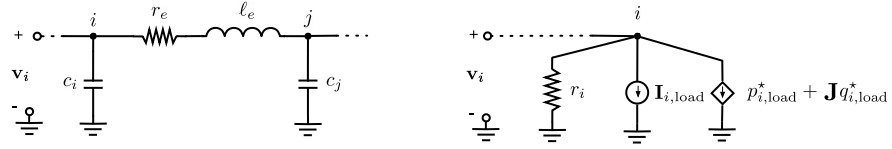


Figure 1

II-model of a power line and schematic illustration of a ZIP load

$\mathbf{I}_{i,\text{load}}^*$ or constant active and reactive power, i.e., $p_{i,\text{load}} = \mathbf{I}_{i,\text{load}}^\top \mathbf{v}_i$ and $q_{i,\text{load}} = \mathbf{I}_{i,\text{load}}^\top \mathbf{J} \mathbf{v}_i$:

$$\mathbf{I}_{i,\text{load}} = \frac{1}{r_i} \mathbf{v}_i + \mathbf{I}_{i,\text{load}}^* + \frac{1}{\|\mathbf{v}_i\|^2} (p_{i,\text{load}} \mathcal{I} + q_{i,\text{load}} \mathbf{J}) \mathbf{v}_i, \quad 7.$$

see Figure 1. Such loads are colloquially termed ZIP loads, where Z, I, and P stand for the impedance, current, power contributions, and many variations thereof have been proposed.

The network model given by equations 1.-7. in dq coordinates reads compactly as

$$\begin{bmatrix} \mathbf{L} \frac{d}{dt} \mathbf{i} \\ \mathbf{C} \frac{d}{dt} \mathbf{v} \end{bmatrix} = \begin{bmatrix} -\mathbf{Z} & \mathbf{B}^\top \\ -\mathbf{B} & -\mathbf{G}(\mathbf{v}) \end{bmatrix} \begin{bmatrix} \mathbf{i} \\ \mathbf{v} \end{bmatrix} + \begin{bmatrix} 0 \\ \mathbf{I}_g - \mathbf{I}_{\text{load}}^* \end{bmatrix}, \quad 8.$$

where we eliminated the voltage drops \mathbf{u}_e ; \mathbf{i} and \mathbf{v} are vectors collecting \mathbf{i}_e and \mathbf{v}_i ; \mathbf{I}_g and $\mathbf{I}_{\text{load}}^*$ are vectors collecting all generation inputs and constant current loads; and we lumped the circuit and load parameters into the diagonal matrices $\mathbf{L} = \text{diag}(l_e \mathcal{I})$, $\mathbf{C} = \text{diag}(c_i \mathcal{I})$, $\mathbf{Z} = \text{diag}(r_e \mathcal{I} + \mathbf{J} \omega_0 l_e)$, and $\mathbf{G}(\mathbf{v}) = \text{diag}\left(\frac{1}{r_i} \mathcal{I} + \frac{1}{\|\mathbf{v}_i\|^2} (p_{i,\text{load}} \mathcal{I} + q_{i,\text{load}} \mathbf{J})\right)$.

The network model 8. is directly amenable to a graph-theoretic (18) or passivity analysis (19). To offer a glimpse into the latter, consider the network power balance

$$\underbrace{\frac{d}{dt} \left(\frac{1}{2} \mathbf{i}^\top \mathbf{L} \mathbf{i} + \frac{1}{2} \mathbf{v}^\top \mathbf{C} \mathbf{v} \right)}_{\frac{d}{dt} \text{ stored energy}} = \underbrace{\begin{bmatrix} \mathbf{i} \\ \mathbf{v} \end{bmatrix}^\top \begin{bmatrix} -\text{diag}(\mathbf{J} \omega_0 l_e) & \mathbf{B}^\top \\ -\mathbf{B} & -\text{diag}\left(\frac{1}{\|\mathbf{v}_i\|^2} q_{i,\text{load}} \mathbf{J}\right) \end{bmatrix} \begin{bmatrix} \mathbf{i} \\ \mathbf{v} \end{bmatrix}}_{= 0 \text{ reactive/circulating power}} \\ - \underbrace{\sum_{i \in \mathcal{V}} p_{i,\text{load}} - \mathbf{v}^\top \mathbf{I}_{\text{load}}^* - \mathbf{v}^\top \text{diag}\left(\frac{1}{r_i}\right) \mathbf{v}}_{\text{active power consumed by loads}} \\ - \underbrace{\mathbf{i}^\top \text{diag}(r_e \mathcal{I}) \mathbf{i}}_{\text{line losses}} + \underbrace{\mathbf{v}^\top \mathbf{I}_g}_{\text{power supplied by generation}}$$

transparently depicting the net-zero contributions from reactive elements, power dissipated by loads and lines, and power supplied by generation sources modeled as current sources $\mathbf{I}_{i,g}$. Section 2.2 below will further specify the modeling of the latter.

2.2. Device-Level Models: Synchronous Machines & Power Converters

Our subsequent discussion of device-level models focuses on synchronous machines and grid-connected power converters, their similarities, as well as their differences.

2.2.1. Synchronous Machine. A synchronous machine converts mechanical to electrical energy by means of a rotating magnetic field inducing torques on the rotor of the machine

and currents on the stator of the machine. We refer to (24) for a comprehensive reference on modeling and to (19) for an intriguing Port-Hamiltonian perspective.

Here, we consider a standard synchronous machine model depicted in Figure 2 and make the following assumptions: the rotor is non-salient, features a single-pole pair, dc-excitation, and no damper windings. The rotor with rotational inertia M , damping D , it is driven by

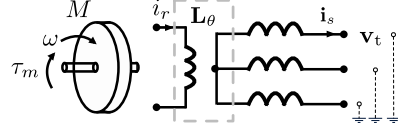


Figure 2

Illustration of a synchronous machine

the (controllable) torque τ_m from the turbine/governor, and its state variables are the angle θ and angular velocity ω . The energy stored in the rotating magnetic field is

$$W = \frac{1}{2} \begin{bmatrix} \mathbf{i}_s \\ i_r \end{bmatrix}^\top \mathbf{L}_\theta \begin{bmatrix} \mathbf{i}_s \\ i_r \end{bmatrix}$$

where \mathbf{i}_s and i_r are the three-phase (in abc) stator and dc rotor flux currents, and

$$\mathbf{L}_\theta = \begin{bmatrix} L_s & 0 & 0 & L_m \cos(\theta) \\ 0 & L_s & 0 & L_m \cos(\theta - \frac{2\pi}{3}) \\ 0 & 0 & L_s & L_m \cos(\theta + \frac{2\pi}{3}) \\ L_m \cos(\theta) & L_m \cos(\theta - \frac{2\pi}{3}) & L_m \cos(\theta + \frac{2\pi}{3}) & L_r \end{bmatrix}$$

is the inductance matrix with the stator, rotor, and mutual inductances L_s , L_r , and L_m . The mechanical dynamics are then (in a frame rotating with ω_0) described by

$$\frac{d\theta}{dt} = \omega - \omega_0 \quad \text{and} \quad M \frac{d\omega}{dt} = -D\omega + \tau_m - \tau_e,$$

where $\tau_e = \frac{\partial W}{\partial \theta}$ is the air gap torque. The damping D due to mechanical and electrical losses is negligible, and often D models the equivalent load damping and damping due to damper windings. The flux linkage equations are then (in abc coordinates)

$$\frac{d}{dt} \left(\mathbf{L}_\theta \begin{bmatrix} \mathbf{i}_s \\ i_r \end{bmatrix} \right) = \begin{bmatrix} -R_s \mathcal{I} & \\ & -R_r \end{bmatrix} \begin{bmatrix} \mathbf{i}_s \\ i_r \end{bmatrix} + \begin{bmatrix} \mathbf{v}_t \\ u_r \end{bmatrix},$$

where R_s and R_r are resistive losses in the stator and rotor coils, u_r is the controllable dc rotor excitation voltage, and \mathbf{v}_t is the three-phase terminal voltage.

When formulating these equations in a dq frame rotating with ω_0 and assuming tight control via u_r of i_r to a reference input (also denoted by i_r for simplicity), we arrive at the air gap torque $\tau_e = L_m i_r \begin{bmatrix} -\sin \theta \\ \cos \theta \end{bmatrix}^\top \mathbf{i}_s$, the induced voltage $\mathbf{v}_{\text{ind}} = L_m i_r \begin{bmatrix} -\sin \theta \\ \cos \theta \end{bmatrix} \omega$, and thus

$$\begin{aligned} \frac{d\theta}{dt} &= \omega - \omega_0 \\ M \frac{d\omega}{dt} &= -D\omega + \tau_m - L_m i_r \begin{bmatrix} -\sin \theta \\ \cos \theta \end{bmatrix}^\top \mathbf{i}_s \\ L_s \frac{d\mathbf{i}_s}{dt} &= -(R_s \mathcal{I} + \mathbf{J} \omega_0 L_s) \mathbf{i}_s + L_m i_r \begin{bmatrix} -\sin \theta \\ \cos \theta \end{bmatrix} \omega - \mathbf{v}_t. \end{aligned} \tag{9}$$

The assumptions underlying the model 9. can be lifted (25), but this model suffices for our discussion. Depending on whether the synchronous machine supplies or absorbs power, it is referred to as a *synchronous generator* (SG) or motor. We investigate the former here.

For latter reference, we note that one normally models the (relatively slow) mechanical actuation via the turbine/governor system on τ_m through a series of linear filters (typically low-pass but sometimes featuring also unstable zeros (23)) giving rise to a delay and sometimes inverse response dynamics. Stability of multi-machine power systems typically leverages reduced-order linearized synchronous machine and turbine models (see the sidebar entitled *Reduced-order synchronous generator and turbine models*).

Reduced-order synchronous generator and turbine models

Low-order approximations of the SG dynamics 9. are commonly used for stability analysis or for gaining qualitative insights into the dynamics. The dynamics of a SG with excitation are commonly represented by the classical *one-axis generator model with exciter* (also known as third-order model), given by (26, 24, 15)

$$\frac{d\theta}{dt} = \omega - \omega_0, \quad 10a.$$

$$\frac{2H}{\omega_0} \frac{d\omega}{dt} = -D\omega + p_m - p_g, \quad 10b.$$

$$T'_{do} \frac{d\|\mathbf{v}_t\|}{dt} = -\|\mathbf{v}_t\| + V_f + \frac{X_d - X'_d}{V_t} q_g, \quad 10c.$$

with scaled inertia constant $H = \frac{M\omega_0}{2S_{base}}$, damping constant D , turbine power p_m , and grid power injection p_g expressed in per unit with base power S_{base} and base frequency ω_0 . Moreover, $\|\mathbf{v}_t\|$ and V_f denote the terminal voltage magnitude and output voltage of the exciter in per unit, T'_{do} denotes the time constant (i.e., ℓ/r) of the excitation winding, and X_d and X'_d denote static and transient d-axis reactances.

Frequency stability is commonly studied using the classical *swing-equation* model obtained by assuming that $\|\mathbf{v}_t\|$ in 10. is constant (i.e., only using 10a. and 10b.). This assumption is commonly justified by the fact that T'_{do} is comparably large (i.e., on the order of seconds (15)). While this prototypical model has proved itself useful (24, 15, 27), its validity has always been a subject of debate; see, e.g., (28, 29, 30).

We emphasize that any SG model needs to be combined with a suitable turbine model. While several specialized models for different turbine technologies exist (see e.g., (15)), the first-order turbine model

$$T_m \frac{dp_m}{dt} = -p_m - K_{gov}\omega \quad 11.$$

with turbine time constant T_m and governor gain K_{gov} is commonly used for analyzing frequency stability and captures the main salient features of the turbine response (31, 10, 27).

2.2.2. DC/AC Voltage Source Converter. A dc/ac power converter converts signals and energy between its dc and ac port. We refer to (16) for a comprehensive modeling reference.

There are many topologies for power electronics conversion. To highlight similarities between SGs and VSCs we consider a basic *voltage source converter* (VSC), as depicted in Figure 3. The VSC converts a dc voltage $v_{dc} \in \mathbb{R}$ and dc current $i_x \in \mathbb{R}$ to a three-phase

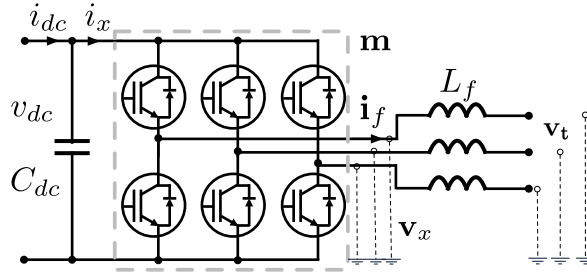


Figure 3
Illustration of a two-level voltage source converter

(in dq coordinates) ac voltage v_x and current \mathbf{i}_f (entering an inductive filter) according to

$$i_x = \frac{1}{2} \mathbf{m}^\top \mathbf{i}_f \quad \text{and} \quad \mathbf{v}_x = \frac{1}{2} \mathbf{m} v_{dc}, \quad 12.$$

where $\mathbf{m} \in [-1, 1] \times [-1, 1]$ are the *averaged* duty cycle ratio (16, Ch. 5). This results in the averaged open-loop model

$$\begin{aligned} C_{dc} \frac{dv_{dc}}{dt} &= -G_{dc} v_{dc} + i_{dc} - \frac{1}{2} \mathbf{m}^\top \mathbf{i}_f \\ L_f \frac{d\mathbf{i}_f}{dt} &= -(R_f \mathcal{I} + \mathbf{J} \omega_0 L_f) \mathbf{i}_f + \frac{1}{2} \mathbf{m} v_{dc} - \mathbf{v}_t \end{aligned} \quad 13.$$

where all parameters are as in Figure 3, G_{dc} and R_f model the lumped switching, charging, and conduction losses, \mathbf{v}_t is the ac voltage at the VSC terminals, and i_{dc} is the controllable dc-side current typically coming from an upstream converter (32, 33) or storage element.

Aside from an upstream power converter and power source, higher-order converter-interfaced generation (CIG) models consider additionally LC or LCL filters at the ac terminals rather than a single inductor. There are also other converter topologies (i.e., arrangements of the switches in Figure 3), but the modeling is conceptually similar.

2.3. Modeling Fallacies in Low-Inertia Power Systems

The power system – all its components and all of its operation – has been built around the central technology of the SG introduced in Section 2.2.1. A testimonial to this fact is the three-phase ac circuitry which is due to the three-phase generation technology displayed in the SG’s inductance matrix \mathbf{L}_θ . Future *low-inertia* power systems will have a large share of CIGs versus rotational generation, and hence conventional modeling assumptions, analysis, and control need to be revisited. In what follows, we comment on a few peculiarities of low-inertia systems and point out fallacies, where conventional models are misleading.

2.3.1. Time-domain versus quasi-steady-state models. The grid’s circuitry has been derived in 8.. This model is of high-fidelity but also cumbersome to simulate due to grid’s vast size and the different time scales involved, e.g., the mechanical time constant of the SG model 9. is of several orders slower than the circuit model 8.. For these reasons and since the stable passive circuit dynamics 8. are typically not of interest, the power system is usually modeled by differential-algebraic equations (34), where the network 8. is put into

a *quasi steady state* (i.e., a steady state in a dq frame) and line flows are eliminated (25):

$$\mathbf{I}_g - \mathbf{I}_{\text{load}}^* - \mathbf{G}(\mathbf{v}) \cdot \mathbf{v} = \mathbf{Y}\mathbf{v}, \quad 14.$$

where $\mathbf{Y} = \mathbf{B}\mathbf{Z}^{-1}\mathbf{B}^\top$ is the network *admittance matrix*. Further, these equations are formulated in units of power (by left-multiplying them by voltage), loads are typically modeled as constant power (or whatever is convenient for analysis) (35), bus voltages \mathbf{v}_i are modeled as phasors $\mathbf{v}_i \sim \|\mathbf{v}_i\|e^{j\theta_i}$, and often voltages at buses without injections are eliminated, cf. *Kron reduction* (36). The active and reactive power balance at bus i is then

$$\begin{aligned} p_{i,g} - p_{i,\text{load}} &= \sum_{j \in \mathcal{V}} \|\mathbf{v}_i\| \|\mathbf{v}_j\| g_{ij} \cos(\theta_i - \theta_j) + \|\mathbf{v}_i\| \|\mathbf{v}_j\| b_{ij} \sin(\theta_i - \theta_j) \\ q_{i,g} - q_{i,\text{load}} &= \sum_{j \in \mathcal{V}} \|\mathbf{v}_i\| \|\mathbf{v}_j\| g_{ij} \sin(\theta_i - \theta_j) - \|\mathbf{v}_i\| \|\mathbf{v}_j\| b_{ij} \cos(\theta_i - \theta_j) \end{aligned} \quad 15.$$

where $p_{i,g} + \mathbf{J}q_{i,g} = \mathbf{v}_i^\top \mathbf{I}_{i,g}$ is the generator power injection, and g_{ij} and b_{ij} are the lossy and lossless admittances obtained as elements of the admittance matrix $Y = g + \mathbf{J}b$.

The so-called *power flow equations* 15. are the foundation of power system steady-state analysis (25) and optimization (37), and they are typically used in conjunction with the SG model 9. for dynamic simulation, analysis, and control. The pivotal assumption underlying the quasi-steady-state power flow 15. is a time-scale separation (between line and SG dynamics), and thus setting the time-derivatives in 8. to zero, as justified by singular perturbation methods (24). However, such an assumption is flawed with a large share of CIG: the dynamics of converters and their controls operate on a similar time-scale as the line dynamics 8., which can result in resonance phenomena and ultimately instability (5, 1, 38, 39, 9, 40). Hence, either the full dynamic network model 8. has to be taken into account; or one has to be crucially aware of the limitations of quasi-steady-state models 14.-15.. In fact, to avoid instability, power converter controllers are deliberately slowed down or equipped with low-pass filters; see (41, 42, 43, 44, 45) for representative studies.

2.3.2. Similarities and differences of SGs and VSCs. We now highlight the similarities and crucial differences of the SG and VSC devices from the viewpoint of energy conversion (46).

Indeed, both devices can be understood as exchanging power between energy storage elements. The power balance across the SG 9. is given by

$$\underbrace{\frac{d}{dt} \frac{1}{2} M \omega^2}_{\substack{\frac{d}{dt} \text{ mech. energy}}} + \underbrace{\frac{d}{dt} \frac{1}{2} \mathbf{i}_s^\top L_s \mathbf{i}_s}_{\substack{\frac{d}{dt} \text{ magn. energy} \approx 0}} = \underbrace{-R_s \|\mathbf{i}_s\|^2 - D \omega^2}_{\substack{\text{electr. \& mech. losses} \approx 0}} + \underbrace{\tau_m \omega}_{\substack{\text{mech. power}}} + \underbrace{\mathbf{i}_s^\top \mathbf{v}_t}_{\substack{\text{ac power}}}, \quad 16.$$

where the electro-mechanical energy conversion through the rotating magnetic field cancels out. Further, the dissipation and magnetic energy terms are negligibly small, and thus the power balance is dominated by the large mechanical energy stored in the rotor as well as the electrical and mechanical power supply from the grid and the torque/governor system.

The power balance across the VSC 13. is given by

$$\underbrace{\frac{d}{dt} \frac{1}{2} C_{dc} v_{dc}^2}_{\substack{\frac{d}{dt} \text{ dc energy}}} + \underbrace{\frac{d}{dt} \frac{1}{2} \mathbf{i}_f^\top L_f \mathbf{i}_f}_{\substack{\frac{d}{dt} \text{ magn. energy} \approx 0}} = \underbrace{-R_f \|\mathbf{i}_f\|^2 - G_{dc} v_{dc}^2}_{\substack{\text{switching \& conduction losses} \approx 0}} + \underbrace{i_{dc} v_{dc}}_{\substack{\text{dc power}}} + \underbrace{\mathbf{i}_f^\top \mathbf{v}_t}_{\substack{\text{ac power}}}, \quad 17.$$

where the dc-ac conversion through the modulation \mathbf{m} cancels out. Further, the dissipation and magnetic energy terms are typically negligibly small, and thus the power balance is dominated by the charge stored in the dc capacity as well as the ac and dc power supplies.

Hence, from an energy-conversion viewpoint, both devices consist of a “dc storage element” (the rotating mass M or the dc capacitor C_{dc}) fed by a “dc power supply” (either mechanical $\tau_m\omega$ or electrical $i_{dc}v_{dc}$), a lossless “dc-ac conversion” (through the magnetic field L_θ or the modulation \mathbf{m}) to a negligible magnetic storage element and eventually the grid power supply ($\mathbf{i}_s^\top \mathbf{v}_t$ or $\mathbf{i}_f^\top \mathbf{v}_t$); see Figure 4 for an illustration.

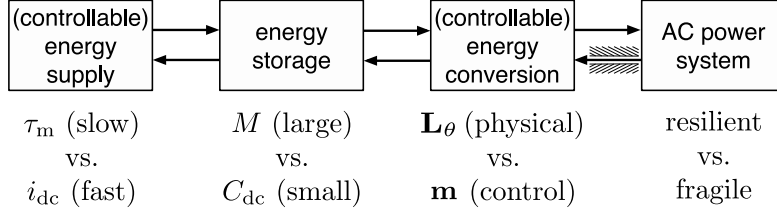


Figure 4

Illustration of the VSC and the SG as energy exchanging and dc-ac signal transforming devices

To further highlight the structural similarities, we parameterize the modulation \mathbf{m} as

$$\mathbf{m} = u_{\text{mag}} \begin{bmatrix} -\sin \delta \\ \cos \delta \end{bmatrix} \quad \text{and} \quad \dot{\delta} = u_{\text{freq}}, \quad 18.$$

where $u_{\text{freq}} \in \mathbb{R}$ and $u_{\text{mag}} \in [-1, +1]$ are the controllable switching frequency and magnitude. With such a polar coordinate representation the VSC dynamics 13. then read as

$$\begin{aligned} \frac{d\delta}{dt} &= u_{\text{freq}} \\ C_{dc} \frac{dv_{dc}}{dt} &= -G_{dc}v_{dc} + i_{dc} + \frac{1}{2}u_{\text{mag}} \begin{bmatrix} -\sin \delta \\ \cos \delta \end{bmatrix}^\top \mathbf{i}_f \\ L_f \frac{d\mathbf{i}_f}{dt} &= -(R_f + \mathbf{J}\omega_0 L_f)\mathbf{i}_f + \mathbf{v}_g - \frac{1}{2}u_{\text{mag}} \begin{bmatrix} -\sin \delta \\ \cos \delta \end{bmatrix} v_{dc}, \end{aligned} \quad 19.$$

The VSC dynamics 19. now take an identical structure as the SG dynamics 16. after associating the dc voltage v_{dc} and capacitance C_{dc} with the SG rotational frequency ω and inertia M . The duality of mass and capacitance is well known to any engineering student, and it has informed multiple VSC control designs (2, 47, 48, 49, 50, 51); cf., Section 3.4.4.

Despite these similarities, a closer look reveals several glaring and crucial differences. Namely, for SGs (resp., VSCs) the actuation via the “dc power supply” is rather slow and inflexible (resp., very fast and flexible), the main “dc storage element” is very large (resp., rather small), the “dc-ac conversion” is mostly physical with little excitation control (resp., fully controlled via the modulation), and the grid-connection is resilient (resp., fragile), i.e., the converter’s switches cannot tolerate any over-current. For these reasons, among others, it is shortsighted for VSC control to emulate a SG in closed loop, c.f., Section 3.4.2.

In short, both devices are dc-ac signal and power transformers; the SG has large inherent energy storage but slow actuation; and the VSC is fully and quickly actuated but without significant storage. These similarities and differences inform the control design in Section 3.

2.3.3. Lingua franca between power systems and electronics. We close this section with some high-level thoughts. Until recently, power systems and power electronics engineers

had few interactions and often spoke different languages. This fact is exemplified by how the two communities used to model each other's systems and devices. In the vast majority of scientific articles and teaching material in power electronics, the considered power system model is simply a stiff voltage source. Vice versa, in the power system world, power converters have been typically modeled as constant or controllable current/voltage/power sources. Aside from the little interaction between the communities, this mutual disregard is simply due to the fact that there was no demand: the physics had little relevant interaction, and there were few operational requirements at the interface. However, as increasingly many CIG sources were connected to the power system, various undesired phenomena emerged on both the grid side (e.g., subsynchronous oscillations) as well as the converter side (e.g., converters not being able to operate in presence of a weak grid or withstand faults).

The authors' beliefs and observations are that control and systems theory can serve as the *lingua franca* translating models and specifications between these two communities. Yet another bridging role of control is to enable CIGs to be *grid-friendly*, as discussed next.

3. CONTROL OF GRID-CONNECTED VSCs

In this section we review and broadly categorize prevalent and emerging control algorithms for grid-connected VSCs. In particular, we will focus on the distinction between grid-following (GFL) control and grid-forming (GFM) control and the impact of the two control paradigms on system stability. We will limit the discussion to the two-level VSC shown in Figure 3 with the understanding that the general ideas presented in this section can be extended to more advanced voltage source converter topologies (see e.g., (52)).

3.1. Degrees of freedom of grid-connected VSCs

Before discussing the control objectives, we review the degrees of freedom of grid-connected two-level VSCs that inform their control objectives and design. Considering the modulated voltage and current 12., the active power supplied by CIG satisfies

$$p_x = \mathbf{i}_f^\top \mathbf{v}_x = \mathbf{i}_f^\top \frac{1}{2} \mathbf{m} v_{dc} = \frac{1}{2} \mathbf{m}^\top \mathbf{i}_f v_{dc} = i_x v_{dc}, \quad 20.$$

and, using $p_{dc} = v_{dc} i_{dc}$ the dc capacitor charge dynamics in 13. can be rewritten as

$$\frac{d}{dt} \frac{1}{2} C_{dc} v_{dc}^2 = -G_{dc} v_{dc}^2 + p_{dc} - p_x. \quad 21.$$

In other words, the dc energy $E_{dc} = \frac{1}{2} C_{dc} v_{dc}^2$ can be directly controlled through the dc power p_{dc} and/or active power p_x . In contrast, $q_x = \mathbf{i}_f^\top \mathcal{J} \mathbf{v}_x$ corresponds to currents that circulate through the switches and ac phases but do not reach the dc side (i.e., are orthogonal to \mathbf{v}_x). Note that a two-level VSC can only modulate ac voltages with magnitude $\|\mathbf{v}_x\| \leq \frac{1}{2} v_{dc}$ and needs to be able to impose voltage magnitudes $\|\mathbf{v}_x\| \geq \|\mathbf{v}_g\|$ to fully control its power injection (see 15.). In this case, the reactive power q_g can be controlled without affecting dc voltage v_{dc} because $q_x = \mathbf{i}_f^\top \mathcal{J} \mathbf{v}_x$ corresponds to currents that circulate through the switches and ac phases but do not reach the dc side (i.e., \mathbf{i}_f is orthogonal to \mathbf{v}_x). Moreover, assuming a lossless filter in quasi-steady-state, p_x and q_x are equal to the grid power injections $p_g = \mathbf{i}_f^\top \mathbf{v}_t$ and $q_g = \mathbf{i}_f^\top \mathcal{J} \mathbf{v}_t$ given by the power flow equations 15..

3.2. Control objectives and control paradigms

We now provide an overview of control objectives and paradigms for grid-connected VSCs.

3.2.1. Control objectives. Before presenting common control objectives, we note that there is no precise and universally agreed upon framework for dynamic specifications for grid-connected VSCs. Instead, control objectives for grid-connected VSCs are commonly formulated in terms of decentralized stabilization (i.e., using only local measurements) of a *nominal steady state* specified by

- *synchronous frequency* (24, 53): all ac signals are balanced periodic three-phase signals with nominal frequency ω_0 ;
- *power injection* (54, 45): each VSC injects the prescribed active and reactive power, i.e., $(p_g, q_g) = (p_g^*, q_g^*)$;
- *ac voltage magnitude* (24, 55): given a nominal ac voltage magnitude V_t^* , it holds that $\|\mathbf{v}_t\| = V_t^*$; and
- *dc voltage* (47, 33): given a nominal dc voltage v_{dc}^* , it holds that $v_{dc} = v_{dc}^*$.

We emphasize that the nominal operating point $(\omega_0, v_{dc}^*, p_g^*, q_g^*, V_t^*)$ needs to correspond to a steady state of the power network, power conversion (e.g., SGs and VSCs), and power generation (53, 56). For example, the power injections (p_g^*, q_g^*) and voltage magnitude V_t^* need to be consistent with the ac power flow equations 15. (see e.g., (25)). Typically, the operating point may be (partially) prescribed by a system operator based on solutions of an *optimal power flow* (56) or local control objectives such as *maximum power point tracking* (MPPT) for renewable generation (32, 33). However, due to disturbances (i.e., variations in load or generation or faults), the nominal operating point may not correspond to an equilibrium of the power system. For example, considering the power balance 16., it can be seen that the frequency will deviate due to mismatches in load and generation. Overall, one or more of the signals needs to deviate from the nominal operating point to stabilize the VSC and overall system at a *synchronous solution* with identical non-nominal frequency at every bus (i.e., $\omega_1 = \omega_2 = \dots = \omega_n$) with minimal transients (24, 57, 58).

Next, we focus on common specifications for the *steady-state disturbance response*. Historically, a large part of the literature focuses on controlling the dc voltage v_{dc} to a setpoint v_{dc}^* (e.g., the maximum power point of photovoltaics (33) or the nominal voltage of a HVDC cable (59)) at all times. In this case, the current i_{dc} or power p_{dc} is treated as an exogenous input (e.g., renewable generation operating at its *maximum power point* (MPP) (32, 33), current flowing into a high voltage dc (HVDC) network (59)). Crucially, if p_{dc} is an exogenous input, the dc voltage dynamics 21. can be controlled only through $p_x \approx p_g$, i.e., the active power p_g is largely prescribed by the dc source power p_{dc} .

In contrast, for VSCs providing grid-support (60), the *steady-state disturbance response* is typically designed to mimic the steady-state droop response of the classical SG turbine (.cf. 11.) and SG excitation system (c.f. 10c.). This results in the so-called *frequency-watt droop* (54, 57) and *volt-var droop* (54, 55)

$$\omega - \omega_0 = m_p \cdot (p_g^* - p_g) \quad \text{and} \quad \|\mathbf{v}_t\| - V_t^* = m_q \cdot (q_g^* - q_g) \quad 22.$$

that trade-off ac voltage frequency and magnitude deviations with active and reactive power deviations according to the droop coefficients m_p and m_q (54). If *frequency-watt droop* is used, it is commonly assumed that the dc voltage v_{dc} is stabilized through controlling the VSC power source (i.e., p_{dc}). Irrespective of how v_{dc} is controlled, the reactive power q_g can be varied within the converter power limits (16, 54).

We emphasize that grid-supporting VSC controls are designed to mimic the response of the classical third-order SG model 10., and the specifications presented in this section are

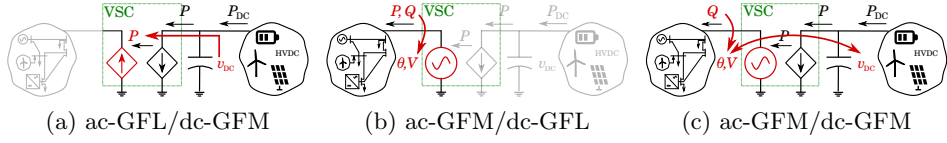


Figure 5

Signals imposed/controlled by the VSC (red) and components neglected in the control design (grey) for (a) typical ac-GFL/dc-GFM control, (b) typical ac-GFM/dc-GFL control, and (c) ac-GFM/dc-GFM control, respectively.

obtained by reverse engineering this response. To the best of the authors' knowledge, dispatchable virtual oscillator control (see Section 3.4.3) is the only principled control approach designed starting from precise specifications (61, 45).

3.2.2. Control paradigms. In the literature control strategies for grid-connected VSCs are typically categorized as *grid-following* (GFL) and *grid-forming* (GFM). We emphasize that there is no precise and universally agreed upon definition of GFM and GFL across different research communities. According to early definitions used in *power electronics* a GFM VSC acts as a voltage source, i.e., it imposes an ac voltage with constant nominal amplitude and frequency, while a GFL VSC acts as current or power source, i.e., it injects a controllable power (54). Nowadays GFM often refers to a VSC that imposes an ac voltage with frequency that is adjusted to ensure frequency synchronization and provide grid-support. In contrast, GFL is often used to describe a VSC that relies on a so-called phase-locked loop (PLL) for synchronization and current control irrespective of whether further grid-support functions are implemented (62). Other definitions encountered in the power systems literature hinge on the presence of virtual inertia, the ability of the VSC to operate islanded with load, or the ability to suppress frequency oscillations (63). While the classification into GFM and GFL commonly refers to the converter ac terminal, it is also useful to characterize a VSC as dc-GFM (resp., dc-GFL) if it imposes (resp., relies on) a stable dc voltage (59).

To highlight the main distinction between GFL and GFM control, we will refer henceforth to a VSC as ac-GFM (resp., dc-GFM) if it imposes a stable well-defined ac (resp., dc) voltage at the ac (resp., dc) converter terminal, and ac-GFL (resp., dc-GFL) if the control crucially hinges on the *assumption* that a well-defined ac (resp., dc) voltage at the VSC ac (resp., dc) terminal is *guaranteed a-priori* by the presence of other generation units. Prototypical implementations of standard ac-GFL/dc-GFM and ac-GFM/dc-GFL control, as well as recently developed ac-GFM/dc-GFM control are shown in Figure 5.

3.3. AC grid-following control of VSCs

The prevalent control for grid-connected renewable generation and energy-storage today is ac-GFL control that uses a PLL (i.e., a PI-type observer) to estimate the terminal voltage phase angle $\angle \mathbf{v}_t$ (see e.g., (64)) and control the VSC current \mathbf{i}_f in the corresponding dq -frame (32, 33, 54). Specifically, the current \mathbf{i}_f is controlled through feedback linearization (i.e., $\mathbf{m} = \frac{2}{v_{dc}} \mathbf{v}_x^*$) and proportional-integral (PI) control, denoted by $G_{PI}(s)$, (54, 65)

$$\mathbf{v}_x^* = (R_f \mathcal{I} + \mathbf{J} \omega_0 L_f) \mathbf{i}_f + \mathbf{v}_t + G_{PI}(s) (\mathbf{i}_f^* - \mathbf{i}_f) \quad 23.$$

such that, with a slight abuse of notation, the closed-loop filter current dynamics 13. become $L_f \frac{d\mathbf{i}_f}{dt} = G_{PI}(s) (\mathbf{i}_f^* - \mathbf{i}_f)$. This PLL-based current control requires (i) a strongly coupled ac system to ensure that the VSC terminal voltage $\mathbf{v}_t = \mathbf{v}_g$ is largely independent of the converter current \mathbf{i}_f (see e.g., (65), (16, Ch. 8)) as well as (ii) ac-GFM units that impose stable ac voltage wave forms. In practice, these assumptions are often questionable and jeopardize system reliability and resilience. In particular, various instability mechanisms ranging from frequency instability to positive feedback induced by the PLL can arise (65, 5). To the best of the authors knowledge analytic stability certificates for ac-GFL have not been extended beyond the setting of VSCs without dc side dynamics connected to an infinite bus, see e.g., (65, 66). Nonetheless, the PLL-based current control is the basis for prototypical ac-GFL/dc-GFM controls used to control the dc voltage of VSCs interfacing renewable generation (32, 33) and HVDC transmission (59). Specifically, considering the dc capacitor dynamics 21., the current \mathbf{i}_f^{d*} and active power $p_x \approx \|\mathbf{v}_g\| \mathbf{i}_f^{d*}$ flowing out of the dc-link capacitor can be used to control the dc voltage (32, 33).

Finally, a wide body of literature exists on ac-GFL/dc-GFL controls that assume a constant dc voltage and compute the current reference \mathbf{i}_f^* using $\mathbf{i}_f^{d*} = p_g / \|\mathbf{v}_g\|$, $\mathbf{i}_f^{q*} = q_g / \|\mathbf{v}_g\|$, as well as p_g and q_g obtained from the droop characteristic 22. and PLL estimates of the grid frequency and ac voltage magnitude (54, 67). However, in the view of the authors and an ever-growing part of the community, ac-GFL/dc-GFL control does not offer any advantage over the ac-GFM/dc-GFL controls discussed in the next section while inheriting the aforementioned stability and resilience concerns related to the PLL (65, 60, 62).

3.4. AC grid-forming control of VSCs

In contrast to the ac-GFL control discussed in the previous section, ac-GFM power converters contribute to grid stabilization and are envisioned to be the cornerstone of future sustainable, reliable, and resilient low-inertia power systems (1, 62, 9). However, the prevalent ac-GFM control methods may fail if the dc voltage is not tightly controlled by the dc power source (10), i.e., they are dc-GFL. In this section, we will discuss ac-GFM control architectures with and without inner control loops, and we will discuss the similarities and differences between three different classes of ac-GFM controls.

3.4.1. Grid-forming control architectures. Broadly speaking, standard ac-GFM control measures the VSC ac current or ac power and adjusts the VSC ac voltage to achieve the control objectives discussed in Section 3.2.1. To this end, the ac-GFM control either directly adjusts the voltage \mathbf{v}_x modulated by the VSC or provides a reference for the LCL filter voltage that is tracked by an underlying cascaded current and voltage controller, as shown in Figure 6. While direct control of \mathbf{v}_x has received some attention in the literature (68, 69, 51, 47, 62), the vast majority of works uses cascaded proportional integral controls that suppress LCL filter resonances through control of \mathbf{v}_t , increase the bandwidth, and provide a simple surrogate for overcurrent protection by limiting the ac current reference \mathbf{i}_f^* (70, 54, 71, 44, 72). While these features are appealing, it should be noted that the inner control loops need to be carefully tuned to account for the strength of the grid coupling to avoid instability (68, 73, 44). In addition, the time-scale separation of cascaded control loops can result in a loss of control bandwidth and suboptimal response (68, 74).

Moreover, limiting the ac current reference can result in a loss of synchronization or synchronous instability (75, 76, 10) and complicates model reduction (72). The reader is

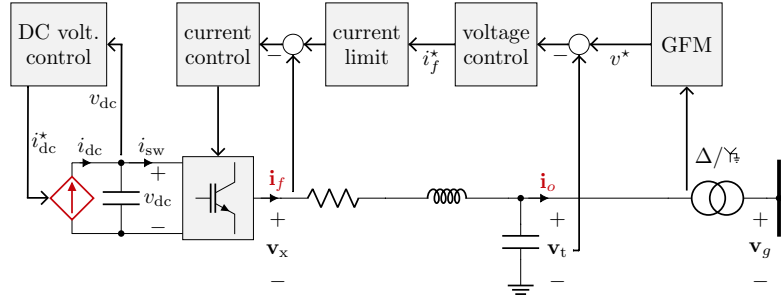


Figure 6

Standard ac-GFM control architecture with cascaded inner loops and controllable dc source.

referred to (77, 75, 76, 78, 72) for an in-depth discussion of current limiting strategies. Next, we focus on the dynamics of the ac-GFM voltage reference \mathbf{v}_{gfm} with the understanding that it can be used with (i.e., $\mathbf{v}_t \approx \mathbf{v}_{\text{gfm}}$) and without (i.e., $\mathbf{v}_x = \mathbf{v}_{\text{gfm}}$) inner controls.

3.4.2. Droop control & virtual synchronous machines. The prevalent approaches to ac-GFM control in the literature are so-called *droop control* (79, 80, 54) and *virtual synchronous machines* (81, 71). Both controls assume a constant nominal dc voltage (i.e., ac-GFM/dc-GFL). Droop control is motivated by the observation that, in steady state, the frequency deviation of the SG is proportional to its active power injection and the voltage magnitude is proportional to its reactive power injection. Moreover, in an inductive network, the active power is approximately proportional to the voltage phase angle differences and reactive power is approximately proportional to voltage magnitude (cf. 15.). In other words, the machine dynamics result in frequency synchronization through the network (57, 82) and active and reactive power sharing (57, 55). Hence, voltage magnitude and frequency *drooping* as in 22. is an integral part of many grid codes.

These observations motivate using feedback of the VSC active power injection p_g to determine the phase angle $\theta = \angle \mathbf{v}_{\text{gfm}}$ and frequency of the ac-GFM reference voltage \mathbf{v}_{gfm} and feedback of the VSC reactive power injection q_g to determine its magnitude $\|\mathbf{v}_{\text{gfm}}\|$. In particular, ac-GFM droop control is obtained by letting $H = 0$, $T_m = 0$, and $T'_{\text{do}} = 0$ in the one-axis SG model with exciter 10.. Linearizing the resulting expression at the nominal terminal voltage magnitude (i.e., one per unit) and replacing the SG power injections with lowpass filtered measurements $\tilde{p}_g = \frac{1}{\tau_{\text{lp},s+1}} p_g$ and $\tilde{q}_g = \frac{1}{\tau_{\text{lp},s+1}} q_g$ (e.g., to remove switching harmonics and set the bandwidth to avoid adverse interactions, c.f. Section 2.3.1) gives

$$\frac{d\theta}{dt} = \omega_0 + m_p \cdot (p^* - \tilde{p}_g) \quad \text{and} \quad \|\mathbf{v}_{\text{gfm}}\| = V^* + m_q \cdot (q^* - \tilde{q}_g) \quad 24.$$

with droop gains m_p and m_q , and power setpoints p^* and q^* . While the droop gains are typically prescribed through grid-codes and markets and typically range from 1% to 5%, we note that the equivalent droop gains of the one-axis SG model with exciter are $m_p = 1/(D + K_{\text{gov}})$ and $m_q = X_d - X'_d$. Finally, we note all of the subsequent GFM controllers below will admit an explicit or implicit drooping behavior akin to 24..

Similar to droop control, a wide range of virtual synchronous machine (VSM) controls have been proposed to mimic SG models such as the one-axis model with exciter 10. and swing-equation model (see e.g., (81, 67, 71, 83)). In light of the fast actuation capabilities of

VSCs and typical power sources, emulating the slow response of the turbine and excitation winding would artificially slow down the VSC response. In particular, letting $T_m = 0$ and $T'_{do} = 0$ in the one-axis SG model with exciter 10. and linearizing at the nominal terminal voltage magnitude and replacing q_g with the filtered measurement \tilde{q}_p results in

$$\frac{2H}{\omega_0} \frac{d\omega}{dt} = -D\omega + p^* - p_g, \quad \|\mathbf{v}_{\text{gfm}}\| = V^* + m_q \cdot (q^* - \tilde{q}_g) \quad 25.$$

with *virtual inertia* constant H and damping D . We emphasize that the limited internal energy storage and overload capability of VSCs precludes emulating a significant inertia constant H (10). In addition, most practical implementations of 24. and 25. rely on auxiliary controls (e.g., virtual impedance, PLL-based damping, inner controls) and are not exact analogues to SGs. Finally, we note that ac-GFM droop control 24. and the VSM 25. are identical up to a change coordinates (82) and that the equivalent inertia constant $\frac{2H}{\omega_0} = \tau_p/m_p$ of ac-GFM droop control 24. is typically small (see Figure 7 and, e.g., (84, 82)).

Conceptually, the equivalence between droop control 24., the VSM in 25., and the SG swing equation model 9. ensures a basic level of interoperability between droop-controlled VSCs, VSMs, and SGs. Moreover, in principle, the vast literature on transient stability analysis for reduced-order SG models (see e.g., (85, 86)) can be readily applied to droop controlled VSCs and VSMs. However, despite decades of research, general (almost or semi) global stability results for networks of SGs interconnected through the dynamic network model 8. or the quasi-steady-state model 15. have remained elusive. Standard results for local asymptotic stability typically assume a lossless network (i.e., $g_{ij} = 0$), constant voltage magnitudes, only apply to the trivial (i.e., zero power flow) solution, and they do not extend to a dynamic network model. Notable results include stability conditions for (i) linearizations around the zero power flow solution with network dynamics (43), (ii) for $\tau_p = 0$, the nonlinear quasi-steady-state network model 15. with no losses, and general synchronous solutions (58), and (iii) linearizations around non-trivial operating points, lossy quasi-steady-state network models, and constant voltage magnitudes (87).

3.4.3. Virtual oscillator control. A seemingly independent class of ac-GFM/dc-GFL controls is so-called *virtual oscillator control* (VOC) (88, 89, 90, 91, 92, 61, 45). While initial works on VOC focused on standalone uninterruptible power supplies (88), follow-on works leveraged the self-synchronization of nonlinear oscillators to control networks of single-phase converters (89, 93, 90, 91). More recent works focus on enabling VOC control for three-phase VSCs to track a nominal operating point (61, 45). In contrast to droop control and VSMs, (almost) global synchronization certificates are available for networks of VOC-controlled VSCs (90, 91). Moreover, robust synchronization is observed in practice (90) and averaging VOC over one cycle (93) recovers droop control for resistive networks (54).

However, for all of the above VOC implementation the nominal power injection cannot be dispatched, and the power sharing by the VSCs and their voltage magnitudes are determined by the load and network parameters. This lack of control over the network's operating point is highly problematic in large-scale systems that are coordinated through system-level controls and market mechanisms. This challenge is resolved in the so-called *dispatchable virtual oscillator control* (dVOC) that is a principled control approach combining a harmonic oscillator with a synchronizing feedback and magnitude control (61, 45).

In stationary $\alpha\beta$ coordinates, the dVOC reference voltage v_{gfm} is given by

$$\underbrace{\frac{dv_{\text{gfm}}}{dt}}_{\text{harmonic oscillation at } \omega_0} = \underbrace{\omega_0 \mathcal{J} v_{\text{gfm}}}_{\text{sync. through current}} + \underbrace{\eta [K v_{\text{gfm}} - R(\kappa) \mathbf{i}_o]}_{\text{volt. magnitude control}} + \eta \alpha \Phi(v_{\text{gfm}}) v_{\text{gfm}} \quad , \quad 26.$$

with synchronization gain $\eta \in \mathbb{R}_{>0}$, magnitude control gain $\alpha \in \mathbb{R}_{>0}$,

$$K = \frac{1}{V^* V^*} R(\kappa) \begin{bmatrix} p_g^* & q_g^* \\ -q_g^* & p_g^* \end{bmatrix}, \quad \text{and} \quad \Phi(v_{\text{gfm}}) := \frac{V^* V^* - \|v_{\text{gfm}}\|^2}{V^* V^*}.$$

Here $R(\kappa)$ denotes the 2D rotation matrix and $\kappa := \tan^{-1}(\omega_0 \cdot \ell/r)$ denotes the ℓ/r ratio of the network that is approximately constant for transmission lines at the same voltage level. Dispatchable virtual oscillator control has several appealing features. First, the nominal operating point of dVOC can be defined through setpoints (V^*, p_g^*, q_g^*) as for droop or VSM controllers. Second, almost global stability certificates are available for dynamic networks (cf. 8.) with uniform ℓ/r ratio, LC filter dynamics, and inner control loops that provide bounds on the network connectivity, network loading, and time-scale separation between control loops and the network dynamics (44). Third, dVOC can be understood as a generalization of droop control and VOC to more general networks (see Figure 7 for classifications and implications). In particular, for inductive networks (i.e., transmission systems) and assuming near nominal voltage magnitudes, dVOC resembles droop control (94). In contrast, for resistive networks (i.e., microgrids) and $p_g^* = q_g^* = 0$, dVOC is identical to averaged VOC (61). Notable recent works include *unified virtual oscillator control* (uVOC) that provides ac-GFL functions and fault ride through capabilities (95).

3.4.4. Machine matching and dual-port grid-forming control. So far we have discussed ac-GFM/dc-GFL controls that neglect the dc voltage dynamics (i.e., assume that $v_{\text{dc}} = v_{\text{dc}}^*$). In contrast, so-called *machine emulation* or *machine matching* control (69, 51, 47, 49) leverage the similarities between dc voltage and synchronous machine frequency as indicators of power imbalances (cf., 16. and 17. as well as 9. and 19.). In particular, using $\frac{d\theta}{dt} = \omega$,

$$\omega = k_\omega v_{\text{dc}}, \quad 27.$$

and \mathbf{m} in $\alpha\beta$ coordinates given by $\mathbf{m} = u_{\text{mag}} \begin{bmatrix} -\sin \theta \\ \cos \theta \end{bmatrix}$; cf. Section 2.3.2. Using this control, the SG dynamics 9. and VSC dynamics 13. coincide with inertia constant $M = \frac{C_{\text{dc}}}{k_\omega^2}$, damping constant $D = \frac{G_{\text{dc}}}{k_\omega^2}$, and torque $\tau_m = \frac{i_{\text{dc}}}{k_\omega}$ (47). The relationship between different ac-GFM controls and SGs is illustrated in Figure 7. In contrast to the VSMS discussed above, the two models are exactly structurally equivalent. However, the inertia and damping constant of the equivalent SG is typically significantly smaller than that of a SG with comparable rating and can result in poorly damped dynamics. Moreover, the controller 27. again leads to the challenging problem of analyzing stability of multi-machine systems.

An often overlooked feature of the control 27. is that it is ac-GFM and ensures power balancing between the dc and ac terminal of the VSC by controlling the dc voltage through the ac terminal. The resulting ac-GFM/dc-GFM control can operate if either the ac or dc voltage are stabilized by another ac-GFM or dc-GFM device. In particular, if the dc voltage (ac voltage frequency) is stabilized by a dc-GFM source (ac-GFM) device, then the ac voltage frequency (dc voltage) is also stable. This observation has led to the development

of so-called dual-port GFM control (96, 52) that combine active power droop 24. with a dc voltage droop term (96)

$$\omega - \omega_0 = m_p \cdot (p^* - p_g) + k_\omega \cdot (v_{dc} - v_{dc}^*) \quad 28.$$

that unifies standard functions of ac-GFM (e.g., primary frequency control) and ac-GFL (e.g., maximum power point tracking) control in a single universal controller without mode switching or PLL. Moreover, the dual-port GFM control 28. enables an end-to-end linear stability analysis accounting for ac and dc transmission, SGs and VSCs with and without controlled generation, and generic models of conventional and renewable generation (96).

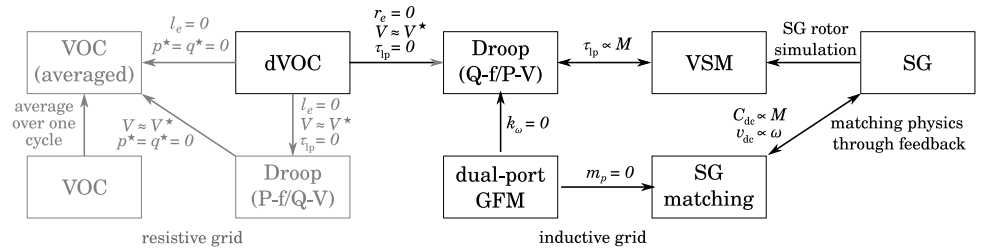


Figure 7
Classification & implications of different ac-GFM controls.

3.5. Grid-forming control as the cornerstone of low-inertia systems

We close this section with some high-level thoughts on the role of ac-GFM and ac-GFL converters in future low-inertia power systems. The two approaches are complementary in the sense that ac-GFM/dc-GFL requires a fully controllable power source (e.g., energy storage) and has a significant positive impact on system stability, damping, and resilience (60, 8, 10, 5, 62), while ac-GFL/dc-GFM requires a stable ac grid (e.g., the presence of ac-GFM units) and stabilizes CIG. Notably, standard ac-GFL control is vulnerable to instability due to grid disturbances (97), weak grid coupling (65), and massive integration of ac-GFL converters (5, 65). On the other hand, at present, ac-GFM control may fail due to limited power source controllability (10) and/or converter current limits (76, 75, 10). Given the clear need for ac-GFM CIG, incorporating converter (e.g., current and modulation limits) and power source dynamics and limitations (e.g., power and bandwidth limits) directly into the design of ac-GFM controls is an important topic for future research. Similarly, MIMO controls that generalize and unify the various ac-GFM approaches and can result in significantly improved dynamic performance (98, 99).

Moreover, at present, a mix of ac-GFL/dc-GFM and ac-GFM/dc-GFL control is needed to operate emerging power systems that contain renewable generation (32, 33) and/or HVDC transmission (59). The resulting complex heterogeneous system dynamics that combine the network dynamics 8., dynamics of the energy conversion devices 9. and 13., dynamics of conventional and renewable generation, as well as ac-GFM and ac-GFL controls, pose significant challenges for power system operation and stability analysis (5). Ultimately, the dynamics of emerging technologies such as HVDC, wind turbines, and energy storage systems (e.g., batteries and flywheels) that are interfaced by VSCs need to be accounted for to certify end-to-end stability (i.e., from power generation to load) instead of merely

certifying stability of a network of ac-GFM converters with constant dc voltage. Machine matching and dual-port GFM controls are a promising approach to tackle this challenge and reduce the system complexity by unifying ac-GFL and ac-GFM control (96).

4. LOW-INERTIA FREQUENCY DYNAMICS & CIG INTEGRATION LIMITS

The previous section focused on control of grid-connected VSCs and the positive impact of ac-GFM control on power system stability and resilience compared to the predominantly negative impact of ac-GFL control. On the other hand, from a practical point of view, the discussion of the transition to a power system with massive integration of CIG often focuses on the so-called loss of rotational inertia due to retiring synchronous generators (100, 3, 4, 7). However, the challenges of this transition related to control and dynamic stability are significantly more nuanced (8, 10, 5). In this section, we briefly review typical models and metrics for frequency dynamics of multi-machine systems, revisit the role of inertia in low-inertia power systems, and discuss open research questions that limit the integration of CIG into today's large-scale systems.

4.1. Frequency stability in multi-machine and low-inertia systems

In power engineering, the frequency dynamics of conventional SG-based power systems are often decomposed into the so-called *center of inertia* (COI) frequency $\omega_{\text{COI}} = \sum_{k=1}^{n_m} H_k / H_{\text{tot}} \omega_k$ with *total system inertia* $H_{\text{tot}} = \sum_{k=1}^{n_m} H_k$, and the deviation of the individual machine angles θ_k and frequencies ω_k from the COI frequency ω_{COI} (24, 27). For homogeneous SGs (i.e., inertia and damping constants are proportional to the SG rating and turbine time constants are identical), the small-signal dynamics of the COI frequency and angle/frequency deviations decouple (27) and can be analyzed in isolation. For brevity of the presentation, we focus on the COI frequency dynamics and refer the reader to (27) for a detailed analysis of the deviation from synchrony. The COI frequency ω_{COI} dynamics are commonly modeled by a single equivalent *swing equation* model (i.e., 10b. with total system inertia $H = H_{\text{tot}}$, negligible damping D and first-order turbine model 11. with aggregate turbine time constant $T_m = T_{\text{agg}}$ (31) and total primary frequency control gain $K_{\text{gov}} = K_{\text{tot}}$ in per unit (24). The response of the COI model 10b. with 11. to a step in active power p_g is shown in Figure 8. From a power engineering point of view, the *rate of change of frequency* (RoCoF) and *frequency nadir* (i.e., its minimum) are key performance metrics. Before proceeding, we emphasize that the COI frequency ω_{COI} is a *fictitious* frequency that

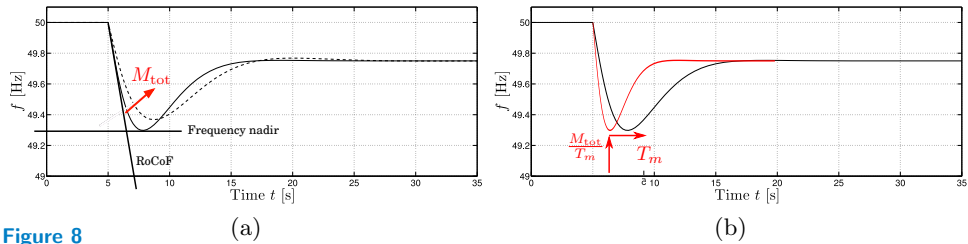


Figure 8 Response of the COI dynamics to a load step. Increasing the inertia H_{tot} results in a decreased RoCoF and frequency nadir (a). A system with larger aggregate turbine time constant T_{agg} evolves on a slower time-scale and increasing the ratio $H_{\text{tot}}/T_{\text{agg}}$ results in a reduced nadir (b).

all SGs would synchronize to in steady state. However, power systems are subject to persistent disturbances (e.g., load fluctuations) and the individual machine frequencies ω_k never settle to the COI frequency ω_{COI} . Thus, ensuring frequency coherency (i.e., small deviations from synchrony) and suppressing inter-area oscillations (see e.g., (101)) are important system-level objectives. Moreover, in systems of heterogeneous SGs the spatial distribution of inertia and damping has a significant impact (see Section 5 for further discussion).

Conventional wisdom suggests that replacing SGs with CIG without virtual inertia results in a reduction of the total inertia H_{tot} and, according to the COI model, an increased RoCoF and frequency nadir (100, 3, 4, 27). However, the kinetic energy stored in the SG rotor merely acts as an energy buffer until the SG turbine responds. Using the ac-GFM controls discussed in the previous section, CIG without virtual inertia responds to power imbalances on the time-scales of milliseconds, i.e., both H_{tot} and the aggregate turbine time constant T_{agg} are reduced. To clarify the impact of this change, note that rescaling time in the COI model does not change the frequency nadir. With $t' = T_{\text{agg}}t$, 10b. and 11. become

$$\frac{2H_{\text{tot}}}{\omega_0 T_m} \frac{d\omega}{dt'} = -D\omega + p_m - p_g \quad \frac{dp_m}{dt'} = -p_m - K_{\text{tot}}\omega. \quad 29.$$

Standard arguments (27) can be used to show that the frequency nadir is a decreasing function of $M_{\text{tot}}/T_{\text{agg}}$. In other words, using ac-GFM CIG, the frequency dynamics of the power system evolve on faster time scales and less inertia is required. While the maximum RoCoF of 10b. scales linearly with H_{tot} , the average RoCoF that is commonly used as a protection signal often improves due to the fast response of ac-GFM CIG (10, 8). Moreover, in a CIG-dominated system a large RoCoF is no longer indicative of a fault, and, in the authors' opinion, its role as protection signal should be reconsidered. Overall, virtual inertia is neither necessary nor a good fit for the VSC characteristics (see Section 2.3.2). Instead, future work should focus on fully leveraging the flexible and fast response of VSCs to overcome fundamental challenges that limit the integration of CIG into large-scale systems.

4.2. CIG Interoperability & Integration Limits

While tremendous progress has been made on control and analysis of CIGs across various spatial and temporal scales the two closely related challenges of characterizing CIG interoperability and integration limits largely remain open. A key challenge is ensuring interoperability of a large number of heterogeneous CIG (possibly using proprietary controls) and conventional SGs through technology agnostic specifications. As of now, the only well understood cases are power systems that solely contain SGs or identical ac-GFM VSCs. For example, analytical results are available for few specific CIG controls and dynamic circuit models (43, 45, 44). Moreover, a stability analysis framework for frequency dynamics of heterogeneous devices interconnected through quasi-steady-state network models has been developed in (102). However, no analytic stability conditions are available that prevent adverse interactions of heterogeneous generation technologies across physics, control, and overlapping time scales. Therefore, interoperability across different technologies and time-scales can, so far, only be studied numerically using high-fidelity simulations and models (103, 104, 8, 5) that may not be available in practice (due to, e.g., proprietary models). Studies along those lines often attempt to frame the problem in terms of a safe CIG integration percentage, or the minimum share of ac-GFM CIG. However, depending on the system topology and controls in question, results can largely differ and numerous adverse interactions between physics and controls of VSCs and SGs as well as the grid dynamics

have been identified (8, 5). We emphasize that the complexity significantly increases if the generation (e.g., wind turbines, solar PV) interfaced by the VSC is accounted for.

Overall, all of the aforementioned studies and results point to the need for stability conditions and analysis tools that are largely agnostic to the underlying technology and grid topology and can be used to ensure interoperability between different generation technologies and better understand fundamental CIG integration limits and system resilience.

5. SYSTEM-LEVEL SERVICES & CONTROL

The previous sections have predominantly focused on the *synchronization* problem, i.e., how to massively integrate CIG in a power system so that the entire system robustly synchronizes. Whereas this task was before naturally accomplished by the SG’s physics, the synchronization of CIGs has to be enabled by means of control. Once synchronized, the next questions concern what CIG should actually contribute to the grid. Ideally, CIG should serve the same roles as rotational generation does nowadays, i.e., provide a (somewhat dispatchable) baseline power injection and grid support similar to SGs: namely, ancillary services supporting voltage and frequency on all time scales but in case of faults also short-circuit current and inertial response – both of which a SG provides by its physical design. This section discusses such system-level stability and control topics in low-inertia systems.

5.1. Dispatch and Allocation of Fast Frequency Response by CIG

Section 4 has introduced performance metrics concerning the power system frequency response, e.g., how non-rotational CIG may (or may not) lead to a larger nadir and steeper RoCoF of the COI frequency following a disturbance. The obvious remedy which has initially been advocated is to provide virtual inertia and/or damping through CIG. This insight is equally obvious and naive since low-inertia issues cannot be fixed by adding the inertia back to the system: partially for device-level reasons already advocated in the previous sections (e.g., see merits and shortages of CIG), but there are also system-level aspects.

The initially prevalent folk theorem that “adding more virtual inertia/damping makes a low-inertia system more robust” has been disproved in many case studies, and nowadays the insight prevails that its careful tuning and spatial allocation over the network has a much more profound impact; see (60, 105, 100, 106, 107, 108) for representative studies. A distilled summary of the conclusions is as follows. (i) The well planned spatial allocation of fast frequency response (i.e., virtual inertia and damping) has a much more profound impact than the total amount. (ii) Heuristic placements (e.g., uniformly across the grid) are rarely optimal but the location of existing rotational generation as well as of faults (or their anticipated probability) needs to be taken into account. In simplified settings, the optimal allocation is actually collocated with the likelihood of faults (105). (iii) Finally, the signal causality (i.e., grid-following or grid-forming implementation) has also profound impacts: grid-following implementations rely primarily on damping (due to a delay incurred by estimating $\frac{d}{dt}\omega$) and are often located near rotational generation, where the PLL-measured frequency is less fluctuating. In contrary, grid-forming CIG are more uniformly allocated.

Further, the choice of cost function strongly affects the allocation of fast frequency response: costs range from spectral criteria placing poles inside a pre-defined damping cone, over specifications on the post-fault response (see Figure 8), to system norms such as \mathcal{H}_2 and \mathcal{H}_∞ ; see (109). As it is well known from the robust control literature, the

system spectrum is often misleading when it comes to transient performance and time-domain specifications are intractable. These considerations make system norms attractive formulations, particularly the computationally tractable \mathcal{H}_2 norm. In this regard, it turns out important to optimize not only performance but also to penalize control effort to obtain economic solutions.

The above insights on spatial allocation of fast-frequency response have by now also led to considerations on the economic side, such as including the spatial allocation in a security-constrained generation dispatch or in virtual inertia markets; see (11, 12, 110, 107).

Finally, the system norm approach to quantify the effect of fast-frequency response, has by now spilled over from the system level to the device level. For example, fast-frequency response design for grid-forming and grid-following converters based on $\mathcal{H}_2/\mathcal{H}_\infty$ approaches has been put forward in (111, 99, 98, 112, 113), among others, and the classification of CIGs into forming and following devices based on system responses has been considered in (63).

5.2. Ancillary Services Distributed Across Distributed Generation

Future power systems will contain an increasing penetration of non-rotational, renewable, and distributed energy resources (DERs). Hence, the reliable provision of ancillary services, as currently ensured by SGs, has to be shouldered by DERs. This imposes great challenges to cope with intermittent renewables, as well as the device-specific limitations of CIGs. A baseline solution are ancillary service markets, where each participating unit has to be able to provide this service. However, often individual units are constrained in terms of power, energy, ramp rates, and so on. As a remedy units are often pooled by aggregators to collectively bid on the market. This concept is known as a *virtual power plant* (114), and it is has been applied to slow and static services such as providing a nominal power injection. Within the scope of this article, we focus on the refined concept of a *dynamic virtual power plant* (DVPP) able to provide dynamic (i.e., fast) ancillary services for low-inertia systems.

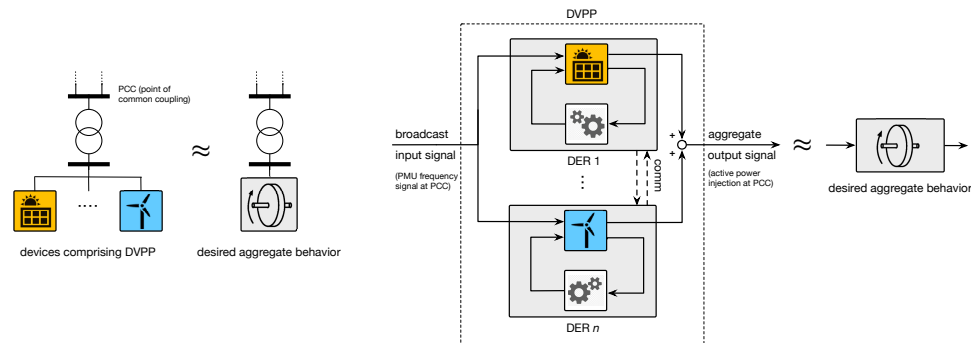


Figure 9

Illustration of a dynamic virtual power plant (DVPP)

A DVPP is a collection of heterogeneous devices (complementing each other in terms of energy/power availability, ramp rates, and weather dependency) that have to be coordinated to collectively provide reliable dynamic ancillary services across all power and energy levels and time scales, while none of the individual devices is able to do so by itself. Examples include hydro-power with initially inverse response dynamics compensated by batteries

on short time scales (115), synchronous condensers (with rotational energy) paired with converter-based generation (116), or hybrid storage pairing batteries with supercapacitors providing regulation on different frequency ranges (117). While for each of these case studies custom solutions have been proposed, an overarching control concept for DVPPs has been recently put forward by (118) and (119, 120), which is schematically illustrated in Figure 9.

To stay with the example from Figure 9, consider a set of generating units connected to the same bus of the high-voltage transmission grid. Consider desired *aggregate specification* on the system level in the form of a dynamic response from a broadcast signal to an aggregate output, e.g., in a grid-following fast frequency response setting a PD-type transfer function (accounting for virtual damping and inertia) from a measured frequency signal to the aggregate power output of all devices. Given such an aggregate specification, the first step is to disaggregate it from the system-level to individual devices, e.g., by broadcasting an error signal (118) to local controllers or customizing it device-by-device via dynamic participation factors (119, 120) (e.g., filtering depending on the devices' power levels and bandwidths). The second step is to match the disaggregated local device-level specifications subject to the device-level constraints, e.g., current limits in case of a CIG. Solutions range from mere tracking control to decentralized, optimal, and adaptive model matching control, accounting for intermittent device capacities and state constraints.

It has been demonstrated in multiple case studies that a DVPP approach brings tremendous improvements over non-coordinated local control actions, and it can match (and sometimes even outperform) the dynamic behavior by SGs. Though, the setup in Figure 9 is of limited scope and has to be extended to the grid-forming and spatially distributed setting.

6. CONCLUSIONS AND OPEN PROBLEMS

In this survey we reviewed modeling and control challenges of low-inertia power systems, both at the device- and system-level, and discussed solutions that have been put forward to date. Overall, we conclude that classical concepts for modeling, stability analysis, simulation, and control of power systems and classical concepts for control of power electronics have to be revisited in light of the transition to low-inertia and converter-dominated power systems. Here, we predominantly focused on novel aspects or traditional concepts which need to be revised in control of low-inertia power systems. Inevitably this article does not present all viewpoints and facets on the topic of low-inertia power systems. For instance, we barely scratched the important roles of markets and policies, energy storage technologies, variability of renewable generation, or demand response to name a few. In all of these aspects, control and optimization play vital roles. It is the authors' firm belief that the system-theoretic mind set is essential to bridge different communities and understand the complex interactions in a power system.

SUMMARY POINTS

1. Control and systems theory can serve as the *lingua franca* translating specifications between power systems and power electronics.
2. The dynamics of synchronous generators and voltage source converters are structurally similar but their limitations and the scales of the parameters differ vastly.
3. AC *grid-forming converters* can replace the fast inertia and slow turbine response of *synchronous generators*. From a control and systems point of view, there is no

- need for an artificial notion of *virtual inertia* as a means of fast frequency response.
4. *Distributed energy resources* need to be coordinated (e.g., in the form of *virtual power plants*) to fully leverage their potential to improve system-level performance.

FUTURE ISSUES

1. Analytical stability certificates need to be developed for *converter-interfaced generation* to overcome *interoperability challenges* and *integration limits* resulting from adverse interactions across spatial / temporal scales and heterogeneous technologies.
2. Advanced grid-forming control needs to explicitly account for the dynamics and constraints of renewable generation, energy storage, and power converters.
3. Grid-forming *dynamic virtual power plants* for spatially distributed *distributed energy resources* are required to fully leverage their potential.

DISCLOSURE STATEMENT

The authors are not aware of any affiliations, memberships, funding, or financial holdings that might be perceived as affecting the objectivity of this review.

ACKNOWLEDGMENTS

This paper is based upon work supported by the European Unions Horizon 2020 research and innovation program (grant agreement No. 883985) and the U.S. Department of Energy (award No. xxx)

LITERATURE CITED

1. Milano F, Dörfler F, Hug G, Hill DJ, Verbič G. 2018. *Foundations and challenges of low-inertia systems*. In *Power Syst. Comput. Conf.*
2. Fang J, Li H, Tang Y, Blaabjerg F. 2018. On the inertia of future more-electronics power systems. *IEEE Trans. Emerg. Sel. Topics Power Electron* 7(4):2130–2146
3. Winter W, Elkington K, Bareux G, Kostevc J. 2015. Pushing the limits: Europe's new grid: Innovative tools to combat transmission bottlenecks and reduced inertia. *IEEE Power and Energy Magazine* 13(1):60–74
4. Tielens P, Hertem DV. 2016. The relevance of inertia in power systems. *Renew. Sust. Energ. Rev.* 55:999–1009
5. Markovic U, Stanojev O, Aristidou P, Vrettos E, Callaway D, Hug G. 2021. Understanding small-signal stability of low-inertia systems. *IEEE Trans. Power Syst.* 36(5):3997–4017
6. Taylor JA, Dhople SV, Callaway DS. 2016. Power systems without fuel. *Renew. Sust. Energ. Rev.* 57:1322–1336
7. Kroposki B, Johnson B, Zhang Y, Gevorgian V, Denholm P, et al. 2017. Achieving a 100% renewable grid: Operating electric power systems with extremely high levels of variable renewable energy. *IEEE Power and Energy Magazine* 15(2):61–73
8. Crivellaro A, Tayyebi A, Gavriluta C, Groß D, Anta A, et al. 2020. *Beyond low-inertia systems: Massive integration of grid-forming power converters in transmission grids*. In *IEEE Power Energy Society General Meeting*

9. Paolone M, Gaunt T, Guillaud X, Liserre M, Meliopoulos S, et al. 2020. Fundamentals of power systems modelling in the presence of converter-interfaced generation. *Electr. Power Syst. Res.* 189:106811
10. Tayyebi A, Groß D, Anta A, Kupzog F, Dörfler F. 2020. Frequency stability of synchronous machines and grid-forming power converters. *IEEE Trans. Emerg. Sel. Topics Power Electron* 8(2):1004–1018
11. Meegahapola L, Mancarella P, Flynn D, Moreno R. 2021. Power system stability in the transition to a low carbon grid: A techno-economic perspective on challenges and opportunities. *Wiley Interdisciplinary Reviews: Energy and Environment* 10(5):e399
12. Mancarella P, Billimoria F. 2021. The fragile grid: The physics and economics of security services in low-carbon power systems. *IEEE Power and Energy Magazine* 19(2):79–88
13. Dörfler F, Bolognani S, Simpson-Porco JW, Grammatico S. 2019. *Distributed control and optimization for autonomous power grids*. In *2019 18th European Control Conference (ECC)*, pp. 2436–2453
14. Kundur P. 1994. *Power System Stability And Control*. McGraw-Hill
15. Machowski J, Lubosny Z, Bialek JW, Bumby JR. 2020. *Power system dynamics: stability and control*. John Wiley & Sons
16. Yazdani A, Iravani R. 2010. *Voltage-sourced converters in power systems: modeling, control, and applications*. John Wiley & Sons
17. Schiffer J, Zonetti D, Ortega R, Stanković AM, Sezi T, Raisch J. 2016. A survey on modeling of microgrids—from fundamental physics to phasors and voltage sources. *Automatica* 74:135–150
18. Dörfler F, Simpson-Porco JW, Bullo F. 2018. Electrical networks and algebraic graph theory: Models, properties, and applications. *Proc. of the IEEE* 106(5):977–1005
19. van der Schaft A, Stegink T. 2016. Perspectives in modeling for control of power networks. *Annual Reviews in Control* 41:119–132
20. Akagi H, Watanabe EH, Aredes M. 2017. *Instantaneous power theory and applications to power conditioning*. John Wiley & Sons
21. Jeltsema D. 2015. *Budeanu’s concept of reactive and distortion power revisited*. In *Int. School on Nonsinusoidal Currents and Compensation*, pp. 1–6
22. O’Rourke CJ, Qasim MM, Overlin MR, Kirtley JL. 2019. A geometric interpretation of reference frames and transformations: dq0, clarke, and park. *IEEE Trans. Energy Convers.* 34(4):2070–2083
23. Kundur PS, Balu NJ, Lauby MG. 2017. Power system dynamics and stability. *Power System Stability and Control* 3
24. Sauer PW, Pai MA, Chow JH. 2017. *Power system dynamics and stability: with synchrophasor measurement and power system toolbox*. John Wiley & Sons
25. GroßD, Arghir C, Dörfler F. 2018. On the steady-state behavior of a nonlinear power system model. *Automatica* 90:248–254
26. Chang HD, Chu CC, Cauley G. 1995. Direct stability analysis of electric power systems using energy functions: theory, applications, and perspective. *Proc. of the IEEE* 83(11):1497–1529
27. Paganini F, Mallada E. 2020. Global analysis of synchronization performance for power systems: Bridging the theory-practice gap. *IEEE Trans. Autom. Control* 65(7):3007–3022
28. Venezian E, Weiss G. 2016. *A warning about the use of reduced models of synchronous generators*. In *Int. Conference on the Science of Electrical Engineering*
29. Monshizadeh P, De Persis C, Monshizadeh N, van der Schaft AJ. 2016. *Nonlinear analysis of an improved swing equation*. In *IEEE Conf. on Dec. and Contr. (CDC)*, pp. 4116–4121
30. Ajala O, Domínguez-García A, Sauer P, Liberzon D. 2020. A library of second-order models for synchronous machines. *IEEE Trans. Power Syst.* 35(6):4803–4814
31. Min H, Paganini F, Mallada E. 2019. *Accurate Reduced Order Models for Coherent Synchronous Generators*. In *Allert. Conf. Commun. Control Comput.*, pp. 316–317
32. Zhou D, Song Y, Blaabjerg F. 2018. Control of wind turbine system. In *Control of Power*

- Electronic Converters and Systems*, ed. F. Blaabjerg, pp. 269–298. Academic Press
33. Teodorescu R, Liserre M, Rodriguez P. 2011. *Grid Converters for Photovoltaic and Wind Power Systems*. Wiley-IEEE Press
 34. Hill DJ, Mareels IM. 1990. Stability theory for differential/algebraic systems with application to power systems. *IEEE Trans. Circuits Syst.* 37(11):1416–1423
 35. Hiskens IA, Hill DJ. 1989. Energy functions, transient stability and voltage behaviour in power systems with nonlinear loads. *IEEE Trans. Power Syst.* 4(4):1525–1533
 36. Dörfler F, Bullo F. 2012. Kron reduction of graphs with applications to electrical networks. *IEEE Trans. Circuits Syst. I* 60(1):150–163
 37. Molzahn DK, Hiskens IA, et al. 2019. A survey of relaxations and approximations of the power flow equations
 38. Misyris GS, Chatzivasilieiadis S, Weckesser T. 2021. Grid-forming converters: Sufficient conditions for rms modeling. *Electr. Power Syst. Res.* 197:107324
 39. Hatziargyriou N, Milanovic J, Rahmann C, Ajarapu V, Canizares C, et al. 2020. Definition and classification of power system stability—revisited & extended. *IEEE Trans. Power Syst.* 36(4):3271–3281
 40. Vorobev P, Huang PH, Al Hosani M, Kirtley JL, Turitsyn K. 2017. High-fidelity model order reduction for microgrids stability assessment. *IEEE Trans. Power Syst.* 33(1):874–887
 41. Raza M, Prieto-Araujo E, Gomis-Bellmunt O. 2017. Small-signal stability analysis of offshore AC network having multiple VSC-HVDC systems. *IEEE Trans. Power Del.* 33(2):830–839
 42. Mariani V, Vasca F, Vasquez JC, Guerrero JM. 2014. Model order reductions for stability analysis of islanded microgrids with droop control. *IEEE Trans. Ind. Electron.* 62(7):4344–4354
 43. Vorobev P, Huang PH, Al Hosani M, Kirtley JL, Turitsyn K. 2017. *A framework for development of universal rules for microgrids stability and control*. In *IEEE Conf. on Dec. and Contr.*, pp. 5125–5130
 44. Subotić I, Groß D, Colombino M, Dörfler F. 2020. A Lyapunov framework for nested dynamical systems on multiple time scales with application to converter-based power systems. *IEEE Trans. Autom. Control* 66(12):5909–5924
 45. Groß D, Colombino M, Brouillon JS, Dörfler F. 2019. The effect of transmission-line dynamics on grid-forming dispatchable virtual oscillator control. *IEEE Trans. Control Netw. Syst.* 6(3):1148–1160
 46. Ortega R, Van Der Schaft AJ, Mareels I, Maschke B. 2001. Putting energy back in control. *IEEE Control Systems Magazine* 21(2):18–33
 47. Arghir C, Jouini T, Dörfler F. 2018. Grid-forming control for power converters based on matching of synchronous machines. *Automatica* 95:273–282
 48. Arghir C, Dörfler F. 2019. The electronic realization of synchronous machines: Model matching, angle tracking, and energy shaping techniques. *IEEE Trans. Power Electron.* 35(4):4398–4410
 49. Li C, Cvetkovic I, Burgos R, Boroyevich D. 2018. *Assessment of virtual synchronous machine based control in grid-tied power converters*. In *Int. Power Electronics Conference*, pp. 790–794
 50. Huang L, Xin H, Wang Z, Wu K, Wang H, et al. 2017. A virtual synchronous control for voltage-source converters utilizing dynamics of dc-link capacitor to realize self-synchronization. *IEEE Trans. Emerg. Sel. Topics Power Electron* 5(4):1565–1577
 51. Curi S, Groß D, Dörfler F. 2017. *Control of low-inertia power grids: A model reduction approach*. In *IEEE Conf. on Dec. and Contr.*, pp. 5708–5713
 52. Groß D, Sánchez-Sánchez E, Prieto-Araujo E, Gomis-Bellmunt O. 2022. Dual-port grid-forming control of MMCs and its applications to grids of grids. *IEEE Trans. Power Del.*
 53. Groß D, Dörfler F. 2017. *On the steady-state behavior of low-inertia power systems*. In *IFAC World Congress*, pp. 10735–10741
 54. Rocabert J, Luna A, Blaabjerg F, Rodríguez P. 2012. Control of power converters in ac mi-

- crogrids. *IEEE Trans. Power Electron.* 27(11):4734–4749
55. Simpson-Porco JW, Dörfler F, Bullo F. 2017. Voltage stabilization in microgrids via quadratic droop control. *IEEE Trans. Autom. Control* 62(3):1239–1253
 56. Capitanescu F, Martinez Ramos J, Panciatici P, Kirschen D, Marano Marcolini A, et al. 2011. State-of-the-art, challenges, and future trends in security constrained optimal power flow. *Electr. Power Syst. Res.* 81(8):1731–1741
 57. Dörfler F, Chertkov M, Bullo F. 2013. Synchronization in complex oscillator networks and smart grids. *Proc. of the National Academy of Sciences* 110(6):2005–2010
 58. Schiffer J, Ortega R, Astolfi A, Raisch J, Sezi T. 2014. Conditions for stability of droop-controlled inverter-based microgrids. *Automatica* 50(10):2457–2469
 59. Gomis-Bellmunt O, Sanchez-Sanchez E, Arevalo-Soler J, Prieto-Araujo E. 2021. Principles of operation of grids of DC and AC subgrids interconnected by power converters. *IEEE Trans. Power Del.* 36(2):1107–1117
 60. Poolla BK, Groß D, Dörfler F. 2019. Placement and implementation of grid-forming and grid-following virtual inertia and fast frequency response. *IEEE Trans. Power Syst.* 34(4):3035–3046
 61. Colombino M, Groß D, Brouillon JS, Dörfler F. 2019. Global phase and magnitude synchronization of coupled oscillators with application to the control of grid-forming power inverters. *IEEE Trans. Autom. Control* 64(11):4496–4511
 62. Lasseter RH, Chen Z, Pattabiraman D. 2020. Grid-forming inverters: A critical asset for the power grid. *IEEE Trans. Emerg. Sel. Topics Power Electron* 8(2):925–935
 63. Debry MS, Denis G, Prevost T. 2019. *Characterization of the grid-forming function of a power source based on its external frequency smoothing capability.* In *IEEE PowerTech*
 64. Chung SK. 2000. A phase tracking system for three phase utility interface inverters. *IEEE Trans. Power Electron.* 15(3):431–438
 65. Dong D, Wen B, Boroyevich D, Mattavelli P, Xue Y. 2015. Analysis of phase-locked loop low-frequency stability in three-phase grid-connected power converters considering impedance interactions. *IEEE Trans. Ind. Electron.* 62(1):310–321
 66. Jafarpour S, Purba V, Johnson B, Dhople S, Bullo F. 2021. Singular perturbation and small-signal stability for inverter networks. *IEEE Trans. Control Netw. Syst.*
 67. Bevrani H, Ise T, Miura Y. 2014. Virtual synchronous generators: A survey and new perspectives. *Int. Journal of Electrical Power & Energy Systems* 54:244–254
 68. Bala S, Venkataramanan G. 2010. *On the choice of voltage regulators for droop-controlled voltage source converters in microgrids to ensure stability.* In *IEEE Energy Conversion Congress and Exposition*, pp. 3448–3455
 69. Cvetkovic I, Boroyevich D, Burgos R, Li C, Mattavelli P. 2015. *Modeling and control of grid-connected voltage-source converters emulating isotropic and anisotropic synchronous machines.* In *IEEE Workshop on Control and Modeling for Power Electronics*
 70. Pogaku N, Prodanovic M, Green TC. 2007. Modeling, analysis and testing of autonomous operation of an inverter-based microgrid. *IEEE Trans. Power Electron.* 22(2):613–625
 71. D’Arco S, Suul JA, Fosso OB. 2015. A virtual synchronous machine implementation for distributed control of power converters in smartgrids. *Electr. Power Syst. Res.* 122:180–197
 72. Ajala O, Lu M, Dhople S, Johnson BB, Dominguez-Garcia A. 2021. Model reduction for inverters with current limiting and dispatchable virtual oscillator control. *IEEE Trans. Energy Convers.*
 73. Qoria T, Gruson F, Colas F, Guillaud X, Debry MS, Prevost T. 2018. *Tuning of Cascaded Controllers for Robust Grid-Forming Voltage Source Converter.* In *Power Syst. Comput. Conf.*
 74. Johnson B, Salapaka S, Lundstrom B, Salapaka M. 2016. *Optimal Structures for Voltage Controllers in Inverters.* In *Int. Symposium on Mathematical Theory of Networks and Systems (MTNS)*, pp. 596–601
 75. Paquette AD, Divan DM. 2015. Virtual impedance current limiting for inverters in microgrids

- with synchronous generators. *IEEE Trans. Ind. Appl.* 51(2):1630–1638
76. Xin H, Huang L, Zhang L, Wang Z, Hu J. 2016. Synchronous instability mechanism of $p - f$ droop-controlled voltage source converter caused by current saturation. *IEEE Trans. Power Syst.* 31(6):5206–5207
 77. He J, Li YW. 2011. Analysis, design, and implementation of virtual impedance for power electronics interfaced distributed generation. *IEEE Trans. Ind. Appl.* 47(6):2525–2538
 78. Groß D, Dörfler F. 2019. *Projected grid-forming control for current-limiting of power converters*. In *Allert. Conf. Commun. Control Comput.*, pp. 326–333
 79. Chandorkar M, Divan D, Adapa R. 1993. Control of parallel connected inverters in standalone ac supply systems. *IEEE Trans. Ind. Appl.* 29(1):136–143
 80. Zhang L, Harnefors L, Nee HP. 2010. Power-synchronization control of grid-connected voltage-source converters. *IEEE Trans. Power Syst.* 25(2):809–820
 81. Zhong QC, Weiss G. 2011. Synchronverters: Inverters that mimic synchronous generators. *IEEE Trans. Ind. Electron.* 58(4):1259–1267
 82. Schiffer J, Goldin D, Raisch J, Sezi T. 2013. *Synchronization of droop-controlled microgrids with distributed rotational and electronic generation*. In *IEEE Conf. on Dec. and Contr.*, pp. 2334–2339
 83. D’Arco S, Suul JA. 2013. *Virtual synchronous machines—Classification of implementations and analysis of equivalence to droop controllers for microgrids*. In *IEEE Powertech*, pp. 1–7
 84. D’Arco S, Suul JA. 2014. Equivalence of virtual synchronous machines and frequency-droops for converter-based microgrids. *IEEE Trans. Smart Grid* 5(1):394–395
 85. Fouad A, Vittal V. 1988. The transient energy function method. *Int. Journal of Electrical Power & Energy Systems* 10(4):233–246
 86. Chiang HD. 2011. *Direct Methods for Stability Analysis of Electric Power Systems: Theoretical Foundation, BCU Methodologies, and Applications*. Wiley
 87. Gholami A, Sun A. 2021. Stability of multi-microgrids: New certificates, distributed control, and braess’s paradox. *IEEE Trans. Control Netw. Syst.*
 88. Aracil J, Gordillo F. 2002. *On the control of oscillations in DC-AC converters*. In *Annual Conference of the Industrial Electronics Society*, vol. 4, pp. 2820–2825
 89. Törres LAB, Hespanha JaP, Moehlis J. 2012. *Power supply synchronization without communication*. In *IEEE Power and Energy Society General Meeting*
 90. Johnson BB, Dhople SV, Hamadeh AO, Krein PT. 2014. Synchronization of parallel single-phase inverters with virtual oscillator control. *IEEE Trans. Power Electron.* 29(11):6124–6138
 91. Törres LAB, Hespanha JaP, Moehlis J. 2015. Synchronization of identical oscillators coupled through a symmetric network with dynamics: A constructive approach with applications to parallel operation of inverters. *IEEE Trans. Autom. Control* 60(12):3226–3241
 92. Johnson BB, Sinha M, Ainsworth NG, Dörfler F, Dhople SV. 2016. Synthesizing virtual oscillators to control islanded inverters. *IEEE Trans. Power Electron.* 31(8):6002–6015
 93. Sinha M, Dörfler F, Johnson BB, Dhople SV. 2017. Uncovering droop control laws embedded within the nonlinear dynamics of van der pol oscillators. *IEEE Trans. Control Netw. Syst.* 4(2):347–358
 94. Seo GS, Colombino M, Subotić I, Johnson B, Groß D, Dörfler F. 2019. *Dispatchable Virtual Oscillator Control for Decentralized Inverter-dominated Power Systems: Analysis and Experiments*. In *IEEE Applied Power Electronics Conference and Exposition*
 95. Awal MA, Husain I. 2021. Unified virtual oscillator control for grid-forming and grid-following converters. *IEEE Trans. Emerg. Sel. Topics Power Electron* 9(4):4573–4586
 96. Subotić I, Groß D. 2022. Power-balancing dual-port grid-forming power converter control for renewable integration and hybrid ac/dc power systems. *IEEE Trans. Control Netw. Syst.*
 97. 2017. 1200 MW fault induced solar photovoltaic resource interruption disturbance report. Tech. rep., NERC
 98. Chen M, Zhou D, Tayyebi A, Prieto-Araujo E, Dörfler F, Blaabjerg F. 2021. Generalized

- multivariable grid-forming control design for power converters. *arXiv:2109.06982*
99. Huang L, Xin H, Dörfler F. 2020. h_∞ -control of grid-connected converters: Design, objectives and decentralized stability certificates. *IEEE Trans. Smart Grid* 11(5):3805–3816
 100. Borsche TS, Liu T, Hill DJ. 2015. *Effects of rotational inertia on power system damping and frequency transients*. In *IEEE Conf. on Dec. and Contr.*, pp. 5940–5946
 101. Winkelman JR, Chow JH, Bowler BC, Avramovic B, Kokotovic PV. 1981. An analysis of interarea dynamics of multi-machine systems. *IEEE Transactions on Power Apparatus and Systems* PAS-100(2):754–763
 102. Pates R, Mallada E. 2019. Robust scale-free synthesis for frequency control in power systems. *IEEE Trans. Control Netw. Syst.* 6(3):1174–1184
 103. Hoke A, Gevorgian V, Shah S, Koralewicz P, Kenyon RW, Kroposki B. 2021. Island power systems with high levels of inverter-based resources: Stability and reliability challenges. *IEEE Electrification Magazine* 9(1):74–91
 104. Kenyon RW, Wang B, Hoke A, Tan J, Antonio C, Hodge BM. 2021. *Validation of Maui PSCAD Model: Motivation, Methodology, and Lessons Learned*. In *North American Power Symposium*
 105. Poolla BK, Bolognani S, Dörfler F. 2017. Optimal placement of virtual inertia in power grids. *IEEE Trans. Autom. Control* 62(12):6209–6220
 106. Pulgar-Painemal H, Wang Y, Silva-Saravia H. 2017. On inertia distribution, inter-area oscillations and location of electronically-interfaced resources. *IEEE Trans. Power Syst.* 33(1):995–1003
 107. Guggilam SS, Zhao C, Dall’Anese E, Chen YC, Dhople SV. 2018. Optimizing der participation in inertial and primary-frequency response. *IEEE Trans. Power Syst.* 33(5):5194–5205
 108. Venkatraman A, Markovic U, Shchetinin D, Vrettos E, Aristidou P, Hug G. 2021. Improving dynamic performance of low-inertia systems through eigensensitivity optimization. *IEEE Trans. Power Syst.* 36(5):4075–4088
 109. Poolla BK, Groß D, Borsche T, Bolognani S, Dörfler F. 2018. Virtual inertia placement in electric power grids. New York, NY: Springer New York, 281–305
 110. Poolla BK, Bolognani S, Li N, Dörfler F. 2020. A market mechanism for virtual inertia. *IEEE Trans. Smart Grid* 11(4):3570–3579
 111. Jiang Y, Pates R, Mallada E. 2020. Dynamic droop control in low-inertia power systems. *IEEE Trans. Autom. Control* 66(8):3518–3533
 112. Tavakoli SD, Fekriasl S, Prieto-Araujo E, Beerten J, Gomis-Bellmunt O. 2021. Optimal h infinity control design for MMC-based HVDC links. *IEEE Trans. Power Del.*
 113. Sanchez-Sanchez E, Gross D, Prieto-Araujo E, Dörfler F, Gomis-Bellmunt O. 2019. Optimal multivariable MMC energy-based control for dc voltage regulation in HVDC applications. *IEEE Trans. Power Del.* 35(2):999–1009
 114. Pudjianto D, Ramsay C, Strbac G. 2007. Virtual power plant and system integration of distributed energy resources. *IET Renewable power generation* 1(1):10–16
 115. Ghasemi H, Melki J. 2019. Investigation of frequency containment reserves with inertial response and batteries
 116. Kenyon RW, Hoke AF, Tan J, Kroposki BD, Hodge BS. 2020. Grid-following inverters and synchr. condensers: A grid-forming pair? Tech. rep., NREL, Golden, CO (United States)
 117. Li W, Joos G. 2008. *A power electronic interface for a battery supercapacitor hybrid energy storage system for wind applications*. In *IEEE Power Electr. Specialists Conf.*, pp. 1762–1768
 118. Zhong W, Chen J, Liu M, Murad MAA, Milano F. 2021. Coordinated control of virtual power plants to improve power system short-term dynamics. *Energies* 14(4):1182
 119. Björk J, Johansson KH, Dörfler F. 2021. Dynamic virtual power plant design for fast frequency reserves: Coordinating hydro and wind. *arXiv preprint arXiv:2107.03087*
 120. Haberle V, Fisher MW, Araujo EP, Dörfler F. 2021. Control design of dynamic virtual power plants: An adaptive divide-and-conquer approach. *IEEE Trans. Power Syst.*